INTERNATIONAL ATOMIC ENERGY AGENCY
UNITED NATIONS EDUCATIONAL, SCIENTIFIC AND CULTURAL ORGANIZATION

INTERNATIONAL CENTRE FOR THEORETICAL PHYSICS
34100 TRIESTE (ITALY) - P.O.B. 586 - MIRAMARE - STRADA COSTIERA 11 - TELEPHONES: 224281/2/3/4/5/6
CABLE: CENTRATOM - TELEX 460392 - I

H4.SMR/164 - 06

WORKSHOP ON CLOUD PHYSICS AND CLIMATE

23 November - 20 December 1985

LECTURES ON GENERAL METEROLOGY

J. Bayo Omotosho
Dept. of Applied Geophysics & Meteorology
Federal University of Technology
Akure, Nigeria

INTERNATIONAL CENTRE FOR THEORETICAL PHYSICS

TRIESTE, ITALY

LECTURES ON

GENERAL METEOROLOGY

by

J. Bayo Omotosho
Department of Applied Geophysics & Meteorology
Federal University of Technology
P.M.B. 704,
AKURE, NIGERIA.

1. ATMOSPHERIC DYNAMICAL AND THERMODYNAMICAL AND PHYSICAL PROCESSES

Weather and Climate occur because air is usually in motion. This motion occurs on a wide range of spectrum both in time and space, from the microscale up to the Rossby waves and the general circulation of the atmosphere. Our understanding of motions on each of these scales relies on the application of some of the physical concepts of hydrodynamics and thermodynamics.

The three basic principles governing the behaviour of the atmosphere are the conservation of (heat) energy, momentum and mass.

Energy conservation allows the study of the way and manner in which the net heat energy from the sun is utilised. In arriving at a balance, cognissance is taken of the roles played by the various gases which make up the atmosphere in effecting short-term physical and thermodynamical changes. By combining the mass and momentum equations with the energy equations, the way and direction of energy transformations in the atmosphere can be studied. This is the aim of this section.

1.1 The Basic Dynamical equations

The first conservation principle is that of momentum. For a non-inertial (relative) frame of reference, it is expressed as

$$\frac{d\underline{V}}{dt} = \underline{g}\cdot\underline{\hat{k}} - 2\underline{\Omega}\wedge\underline{V} - \alpha\nabla p + \underline{F} \qquad \ldots \quad (1.1)$$

where $\underline{V}$ - the velocity relative to the earth with components (u,v,w).

$\underline{g}$ - the gravitational acceleration

$\underline{\hat{k}}$ - a unit vector in the vertical

$\underline{\Omega}$ - the earth's angular velocity

$\underline{F}$ - the frictional force on a unit mass of air

α - specific volume ($= 1/\rho$, ρ is density)

p - the pressure

Since large scale motions in the atmosphere are quasi-horizontal and follow essentially the earth's shape, (1.1) becomes in component form in spherical co-ordinates (λ, ϕ, z):

$$\frac{du}{dt} = -\alpha\frac{\partial p}{\partial x} - \frac{uw}{r} + \frac{uv}{r}\tan\phi - 2w\Omega\cos\phi + fv + F_x$$

$$\frac{dv}{dt} = -\alpha\frac{\partial p}{\partial y} - \frac{vw}{r} - \frac{u^2}{r}\tan\phi - fu + F_y \qquad (1.2a,b,c)$$

$$\frac{dw}{dt} = \frac{u^2+v^2}{r} - \alpha\frac{\partial p}{\partial z} - g + 2u\Omega\cos\phi + F_z$$

λ, ϕ represent longitude and latitude respectively.

Equations (1.2a,b,c) satisfy the angular momentum principle if we ignore the elliptic shape of the earth because the absolute velocity $(u + r\cos\phi)$ is not the true velocity to a non-rotating observer.

When terms of $\lesssim 10^{-3}$ are neglected (e.g. uw/r), the simplified equations are:

$$\frac{du}{dt} = -\alpha\frac{\partial p}{\partial x} + \left(f + \frac{u\tan\phi}{r}\right)v + F_x$$

$$\frac{dv}{dt} = -\alpha\frac{\partial p}{\partial y} - \left(f + \frac{u}{r}\tan\phi\right)u + F_y \qquad (1.3a,b,c)$$

$$0 = -\alpha\frac{\partial p}{\partial x} - g + F_z$$

Furthermore, for flows with Rossby number $R_o\,(=U/fL) \ll 1$, the geostrophic approximation may be obtained from (1.3a,b) as

$$\underline{V}_g = \frac{\alpha}{f}\underline{\hat{k}}\wedge\nabla p \qquad \ldots \quad \ldots \quad (1.4)$$

and (1.3c) leads to the hydrostatic equation

$$g + \alpha \frac{\partial p}{\partial z} = 0 \qquad .. \quad (1.5)$$

or

$$\frac{\partial \Phi}{\partial p} = -\alpha = -\frac{RT}{p} \qquad .. \quad (1.6)$$

where R is the gas constant, T the temperature and Φ the geopotential is given by:

$$\Phi = \int_0^z g\, dz \qquad .. \quad (1.7)$$

An alternative justification for (1.4) comes from consideration of the thermal stratification. When entropy S is used, the Brunt-Vaisala frequency N, may be expressed as:

$$N^2 = \frac{g}{c_p}\frac{\partial S}{\partial z} = \frac{g}{T}\left(\Gamma_d - \gamma\right)$$

where $\Gamma_d = g/c_p$ and $\gamma = -\frac{\partial T}{\partial z}$ are the dry adiabatic and environment lapse rates respectively. c_p is the specific heat at constant pressure. For typical γ of 6.5°C/Km, $N^2 \sim 10^{-4} s^{-2}$ But $\Omega^2 \sim 10^{-9} - 10^{-9} s^{-2}$. Hence $N^2 \gg \Omega^2$

In the tropical and equatorial regions however, (1.3a,b,c) are invalid since $f \gtrsim 10^{-5}$ and hence $R_o \gtrsim 1$. Moreover, dw/dt in and very close to storms can be large ($\sim 0.1 ms^{-2}$) while $w \gtrsim 1 - 10 ms^{-1}$! Thus equation (1.3) is totally unrealistic in the tropics and in such regions where the horizontal scale is less than about 300Km.

The second conservation principle concerns that of mass - the continuity equation. This is

$$\frac{d\rho}{dt} + \rho \nabla . \underline{V} = 0 \qquad .. \quad (1.8)$$

When pressure is the vertical co-ordinate, equation (1.3a,b), with the quadratic and friction terms neglected, become in vectorial form

$$\frac{\partial \underline{V}}{\partial t} = -\nabla \Phi - (\underline{V}.\nabla)\underline{V} - \omega \frac{\partial \underline{V}}{\partial p} - f \underline{k} \wedge \underline{V} \qquad (1.9)$$

The conservation of mass is

$$\nabla . \underline{V} + \frac{\partial \omega}{\partial p} = 0 \qquad .. \quad (10)$$

where $\omega = dp/dt$ and $\omega \approx -\rho g w$, since $u\partial p/\partial x$ etc $\ll w \partial p/\partial z$.

A barotropic atmosphere is one in which there is no change of wind with height. From the thermal wind equation (obtained from (1.4) and (1.6))

$$f \frac{\partial \underline{V}}{\partial \ln p} = -\underline{k} \wedge \nabla \frac{\partial \Phi}{\partial p} \qquad .. \quad (1.11)$$

we must have that

$$\underline{k} . \nabla \frac{\partial \Phi}{\partial p} \equiv \frac{R}{p} \underline{k} \nabla T = 0$$

hence

$$\nabla T = 0$$

The remaining conservation principle is represented by the the First Law of thermodynamics. This will be expressed in terms of the potential temperature θ and entropy S:

$$\frac{dS}{dt} = c_p \frac{d}{dt} \ln \theta = \frac{Q}{T} \qquad .. \quad (1.12)$$

$$\theta = T (1000/p)^k \qquad .. \quad (1.13)$$

where $k = R/c_p$

Q is the diabatic heating rate. If (1.13) is differentiated as in (1.12) and combined with (1.6), we obtain

$$\frac{\partial}{\partial t}\left(\frac{\partial \Phi}{\partial p}\right) = -\underline{V}\cdot\nabla\frac{\partial \Phi}{\partial p} - \frac{kQ}{p} - \frac{\omega}{p}\frac{\partial}{\partial p}\left(p\frac{\partial \Phi}{\partial p} - k\Phi\right) \quad .. \quad (1.14)$$

Equations (1.6), (1.9), (1.10) and (1.14) provide a set of equations for the six unknowns u,v,w,p, ρ and T. They are the so-called primitive equations (Equation of state is implicit in (1.6)).

For mid-latitude synoptic-scale systems, the distribution of the geopotential Φ suffice to determine the fields of the geopotential tendency ($\partial\Phi/\partial t$) and vertical motion ω. This is possible because the mid-latitude atmosphere is baroclinic and significant changes occur in z (or Φ) over short horizontal distances. The tropical atmosphere is, on the other hand, quasi-barotropic. However, the temperature field shows weak (but sufficient) baroclinicity for the geostrophic approximation to be valid down to 10°N (Omotosho, 1976). Nevertheless, existing height fields (or Φ) vary very little and equation (1.14) cannot be used as for the mid - and high latitudes. In tropical areas, the observed wind fields are more reliable than the geopotential heights (Burpee, 1972). This is so because the temperature error inherent in radiosonde element makes it very difficult to analyse the geopotential field in low latitudes from the hydrostatic law. The magnitudes of such errors (1°C error leads to about 20 metres in Φ) are unacceptable as the amplitudes of synoptic scale weather systems in the tropics are rather small.

1.2 Vorticity Consideration

6

In the middle latitudes where the field of Φ suffice to determine $\partial\Phi/\partial t$ and ω, the quasi-geostrophic vorticity equation is very useful instead of the horizontal equations of motion. For a Beta-plane approximation, this is:

$$\frac{\partial}{\partial t}\nabla^2\psi = -\underline{V}_\psi\cdot\nabla(\nabla^2\psi + f) + f_o\frac{\partial \omega}{\partial p} \quad .. \quad (1.15)$$

where

$$\underline{V}_\psi = \underline{\hat{k}}\wedge\nabla\psi \; ; \; \nabla\cdot\underline{V}_\psi = 0 \quad .. \quad (1.16)$$

and

$$\underline{\hat{k}}\cdot\nabla\wedge\underline{V} = \nabla^2\psi = \zeta_g$$

$$f_o\nabla^2\psi = \nabla^2\Phi \quad .. \quad (1.17)$$

ψ is the stream function and $\underline{V}_\psi$ the non-divergent part of $\underline{V}(=V_\psi+V_\chi)$. f_o is a constant value of the coriolis parameter - for motions with small latitudinal scale compared to the earth's radius.

$$\left(u_\psi = -\partial\psi/\partial y \; ; \; v_\psi = \partial\psi/\partial x\right)$$

For these systems, $\psi \simeq \Phi/f_o$ so that $\underline{V}_\psi \simeq \underline{\hat{k}}\wedge\nabla\Phi/f_o$

Also in such motions, $|\nabla\cdot\underline{V}| << |\underline{\hat{k}}\cdot\nabla\wedge\underline{V}|$ since the Rossby number R is small.

In the case of the tropics, the vorticity equation which is found to be very useful and of better approximation to mid-tropospheric synoptic-scale system outside convective or precipitating regions is the so-called Barotropic vorticity equation:

$$\frac{\partial}{\partial t}\nabla^2\psi = -\underline{V}_\psi \cdot \nabla\left(\nabla^2\psi + f\right) \quad .. \quad (1.18)$$

This equation assumes that the flow is quasi-non divergent, but does not require quasi-geostrophy. In this case, the divergence and vorticity may be of same order of magnitude but the latter is usually larger than the divergence. Writing (1.18) in the advective form, neglecting f and integrating over a closed domain σ gives

$$\int \frac{\partial \xi}{\partial t} d\sigma = -\int \nabla\cdot(V_\psi \xi) d\sigma = -\int \xi (\underline{V}_\psi \cdot \hat{\underline{n}}) dL \qquad (1.19)$$

where $\hat{\underline{n}}$ is a unit vector normal to the surface enclosed by L. Denoting the avaraged value of ξ over the domain by $\overline{\xi}$ where

$$\overline{\xi} = \int \xi \, d\sigma \Big/ \int d\sigma$$

in (1.19) leads to a useful conservation properly of the mean vorticity:

$$\frac{\partial \overline{\xi}}{\partial t} = 0 \qquad .. \quad (1.20)$$

It may also be shown (using Gauss's-Div Theorem) after multiplying the simplified (1.18) by ξ that

$$\frac{\partial}{\partial t}\left(\overline{\xi^2}/2\right) = 0 \qquad \left(\xi^2 \text{ is enstrophy}\right) \quad .. \quad (1.21)$$

and that, additionally, the mean kinetic energy $\left(\overline{\nabla\psi\cdot\nabla\psi}/2\right)$ of such flow is also conserved in the domain.

This when advection alone is considered in (1.18), no local time changes in the mean vorticity occurs.

1.3 ENERGY CONSTRAINTS AND CYCLE

A very important link between the momentum conservation principle and the thermodynamic equation is the energy transformation process. This shows how thermal and Kinetic energies are related through a conversion process, to satisfy the energy conservation principle.

The Kinetic energy equation may be easily obtained from (1.19) and (1.10) as

$$\frac{\partial K}{\partial t} + \nabla\cdot\underline{V}K + \frac{\partial}{\partial p}\omega K = -V\cdot\nabla\Phi + \underline{V}\cdot\underline{F} \quad .. \quad (1.22)$$

Multiplying (1.10) by Φ and adding to (1.22) leads, after some rearrangement, to a useful form of the energy equation:

$$\frac{\partial k}{\partial t} + \nabla\cdot\left[\underline{v}(K+\Phi)\right] + \frac{\partial}{\partial p}\left[\omega(K+\Phi)\right] = \omega\frac{\partial\Phi}{\partial p} + \underline{V}.\underline{F} \quad .. \quad (1.23)$$

Again multiplying (1.10) by C_pT and adding the result to the thermodynamic equation gives

$$\frac{\partial h}{\partial t} + \underline{V}\cdot\nabla(\underline{V}h) + \frac{\partial}{\partial p}\omega h = \omega\alpha + Q \quad .. \quad (1.24)$$

where $h = C_pT$ is the enthalpy, or simply potential energy.

Since $\alpha = \partial\Phi/\partial p$ (equation (1.6)), comparision of (1.23) with (1.24) shows that Kinetic energy of motion is produced from potential energy through the term $\omega\alpha\left(= \omega RT/p\right)$. $\omega\alpha$ is commonly referred to as the energy conversion rate.

Integrating (1.23) over the entire atmosphere gives the rate of increase in mean Kinetic energy:

$$\frac{\partial}{\partial t}\int K\,dM = -R\int\frac{\omega T}{p}dM + \bar{F} \qquad .. \quad (1.25)$$

(1.25) states that the direction of Kinetic energy change would depend on the correlation between ω and T. If warm air rises (as on the equatorward side of the Hadley cell) and cold air sinks, there will be an increase in mean Kinetic energy and this, by (1.24), will be at the expense of mean potential energy since $\overline{\omega\alpha} < 0$. Consequently, the Hadley circulation is called a <u>thermally direct</u> cell. (1.25) also implies energy dissipation by frictional forces.

Finally, adding (1.23) and (1.24) gives

$$\frac{\partial}{\partial t}(K+h) + \nabla\cdot\left[\underline{V}(K+\Phi+h)\right] + \frac{\partial}{\partial p}\left[\omega(K+\Phi+h)\right] = Q + \underline{V}\cdot\underline{F} \qquad .. \quad (1.26)$$

Integrating over entire atmosphere with $\omega = 0$ at $p = 0$ and $p = p_s$ (surface) and applying divergence theorem yields

$$-\frac{1}{g}\frac{\partial}{\partial t}\iint(K+h)\,d\sigma\,dp = \bar{Q} + \bar{F} \qquad .. \quad (1.27)$$

Thus the time rate of change of mean total energy is due only to diabatic heating and frictional forces. Hence for adiabatic and frictionless flow

$$\bar{K} + \bar{h} = \text{constant} \qquad .. \quad (1.28)$$

and energy transformations is always between potential and kinetic energies.

Since only a very small fraction $(1\sim2\%)$ of atmospheric potential energy is actually available for conversion into Kinetic energy, <u>the available potential energy, A.</u> (Lorenz, 1967) is introduced and may be expressed as

$$\frac{\partial A}{\partial t} = \frac{\partial}{\partial t}\left[\frac{c_p\Gamma_d\,\widetilde{T''^2}}{2\tilde{T}(\Gamma_d-\tilde{\Gamma})}\right] \qquad .. \quad (1.29)$$

Γ_d is dry adiabatic lapse rate and T" is the departure of temperature from the mean. The energy equations may now be written simply as

$$\frac{\partial A}{\partial t} = g - c \qquad .. \quad (1.30)$$

$$\frac{\partial K}{\partial t} = c - d \qquad .. \quad (1.31)$$

where $g = \Gamma_d\,\widetilde{Q''T''}\Big/\left[\tilde{T}(\Gamma_d-\tilde{\Gamma})\right]$

is the generation (source) of A

c the conversion (sink) of A

d the dissipation of K.

A disadvantage of (1.29) occurs when $\Gamma_d \longrightarrow \tilde{\Gamma}$ a situation frequently met in the low latitudes (Pearce, 1978). Application of the concept to convection in low latitudes is possible from Pearces definition which partitions A into its baroclinicity$(\widetilde{T^{*2}})$ and static stability$(\widetilde{T'^2})$components:

$$\frac{\partial A}{\partial t} = \frac{\partial}{\partial t}\left[\frac{c_p\left(\widetilde{T'^2}+\widetilde{T''^2}\right)}{2\hat{T}}\right] \qquad .. \quad (1.32)$$

where $\hat{T}$ is a global average of T. T' is associated with lapse rate changes only whereas T" is associated with horizontal temperature gradients.

Thus (1.30) and (1.31) each contain terms for zonal and eddy components of the flow. The directions of the complex energy exchanges in the atmosphere is shown in Figure 1.

All the motions, energy exchanges and transfers discussed above would not be possible but for the radiative absorption and transfer which take place between the earth and the atmosphere as a result of constant absorption of solar radiation and the emission of their own radiation to space.

The rate of energy transfer by electromagnetic radiation, the radiant flux F from the sun, is 3.90×10^{26}W. This gives an irradiance E at the outer fringes of the sun ($r \sim 7 \times 10^8$m) of

$$E = F / 4\pi r^2 = 6.34 \times 10^7 \text{ Wm}^{-2}$$

The irradiance E may be defined in terms of the monochromatic irradiance E_λ(irradiance per unit wavelength interval at wavelength λ) as

$$E = \int_0^\infty E_\lambda \, d\lambda \qquad .. \quad (1.33)$$

The radiance I, which is the irrandiance per unit solid angle, is often very useful. E and I are related as

$$E = \int_0^{2\pi} I \cos\phi \, d\omega \qquad .. \quad (1.34)$$

$d\omega$ is the solid angle. $I \cos\phi$ is the component of the radiance normal to the surface at zenith angle ϕ.

A curve of E_λ vs λ is shown in Figure 2.

Figure 2 is also satisfied by Wien's displacement law that the wavelength of peak emission, λ_{max} is higher at lower emmission temperatures:

$$T \lambda_{max} = \text{constant} \qquad . \quad (1.35)$$

The dependence of (blackbody) emission upon temperature is obtained from Plank's Law for monochromatic irradiance at temperature T to give Stefan-boltzmann law:

$$\pi E^* = \sigma T^4 \qquad .. \quad (1.36)$$

where E^* is the integral of Planks equation over all wavelengths, that is,

$$E^* = \int_0^\infty E_\lambda^* = \int_0^\infty \frac{C_1}{\lambda^5 \exp(C_2/\lambda T)}$$

C_1 and C_2 have values 3.74×10^{-16} Wm^{-2} and 1.44×10^{-2} m°K respectively.

The ratio of absorbed to incidence irradiance on a body is known as its absorptivity a_λ while the strength, of the radiation emitted by the body depends on its emissivity ε_λ.

If a body radiates as much heat energy as it absorbs, it is a blackbody. Kirchhoff's Law states that any body which absorbs strongly at a particular wavelength will also radiate strongly at that wavelength. In this case

$$a_\lambda = \varepsilon_\lambda \qquad .. \quad (1.37)$$

Kirchhoff's Law is applicable to the atmosphere below 60km height.

For a non-opaque layer, the incident monochromatic irradiance at any wavelength may be absorbed, reflected or transmitted. Thus

E_λ(absorbed) + E_λ(reflected) + E_λ(transmitted) = E_λ(incident)

Since E_λ(absorbed)/E_λ(incident) = a_λ etc, we have that

$$a_\lambda + \varepsilon_\lambda + \tau_\lambda = 1 \qquad .. \quad (1.38)$$

τ_λ is the transmissivity of the layer. For an opague surface $\tau_\lambda = 0$.

In a plane parallel atmosphere uniform in the horizontal, absorption of radiation in the vertical is given by Beer's (or Lambert's) Law:

$$dE_\lambda = -E_\lambda k_\lambda \rho \, dz \qquad .. \quad (1.39)$$

where k_λ is the absorption coefficient at wavelength λ and is related to the optical depth χ as

$$\chi_\lambda = \int_z^\infty \rho k_\lambda \, dz \qquad .. \quad (1.40)$$

Integration of (1.39) yields

$$E_\lambda = E_{\lambda_0} \exp(-\chi_\lambda) \qquad .. \quad (1.41)$$

Terrestrial Radiation

The foregoing treatment applies to solar radiation through the atmosphere for which atmospheric absorption is important but emission is negligible. Because of the diffuse nature of terrestrial radiation, both emission and absorption are important and calculations usually involve integration over a solid angle. The problem simplifies to a one-dimensional one if we consider the upward and downward fluxes (ie. $\int I(\phi) \cos\phi \, d\omega$) at the downward and upward facing hemispheres. The assumption of course is one of a plane parallel atmosphere. The resulting equation of transfer is then the difference between the emission and the absorption:

$$dI_\lambda = -k_\lambda (\rho I_\lambda - \rho E^*) \qquad .. \quad (1.42)$$

where the blackbody monochromatic emission E^* is given by (1.36). From (1.40), (1.42) may be expressed as

$$\frac{dI_\lambda}{d\chi_\lambda} = I - E^* \qquad . \quad . \quad (1.43)$$

Equation (1.42) or (1.43) is known as the Schwarzchild's equation.

The radiative treatment presented above for both solar and terrestrial assumes a non-scattering atmosphere. This is of course unrealistic since significant scattering of radiation occurs in the atmosphere by air molecules and dust particles. Also, a constant absorption coefficient is assumed which again is not the case since absorber gas concentration varies in the vertical. Major absorbers are water vapour, clouds and ozone.

A more realistic approach is to be able to find the radiation intensity at any given level in the atmosphere with any composition and vertical structure. This is demonstrated by Dugdale under Satellite Meteorology

When the necessary transfer calculations are made, it is then possible to deduce the contribution of radiative processes to the atmospheric energy budget and their role in the conservation laws.

2. INSTABILITY MECHANISMS

Instability processes are very important in the atmosphere because they allow the origin of disturbances on various space and time scales to be determined from the flow thermodynamics and hydrodynamics. Ordinary diagnostic methods of the quasi-geostrophic theory only serve to account for the maintenance of, and relationships between, velocity, pressure and temperature fields.

2.1 Baroclinic Instability

The middle latitude atmosphere is baroclinic and (baroclinic) waves which amplify through the loss of potential energy of the basic flow develop within the zonal flow.

Horizontal temperature advection plays a crucial role in the development of baroclinic waves. Baroclinic instability in zonal flows was studied independently at about same time by Charney (1947) and Eady(1949), the latter providing our present understanding of the origin of cyclone waves while Charney's work dealth with longer waves.

Eady's treatment may be summarised very simply by starting with the simplified vorticity, thermodynamic and continuity equations in x,y,z,t (in which set $R_o << 1$ and f is constant). These are

$$\frac{\partial \xi}{\partial t} + \underline{V}_h \cdot \nabla \xi - f \frac{\partial w}{\partial z} = 0 \quad .. \quad (2.1)$$

$$\frac{\partial s}{\partial t} + \underline{V}_h \cdot \nabla s + wB = 0 \quad .. \quad (2.2)$$

$$\frac{\partial u}{\partial x} + \frac{\partial v}{\partial y} = 0 \quad .. \quad (2.3)$$

The equation satisfied by the perturbation stream function ψ (assumed geostrophic) may be expressed by the single linear equation:

$$\left(\frac{\partial}{\partial t} + U\frac{\partial}{\partial x}\right)\left(\nabla^2\psi + \frac{f^2}{gB}\frac{\partial^2\psi}{\partial z^2}\right) \quad .. \quad (2.4)$$

where

$$B = \frac{1}{\theta}\frac{\partial \theta}{\partial z} \equiv \frac{\partial s}{\partial z}$$

$$\psi = \frac{g}{f}\Delta s \quad .. \quad (2.5)$$

$$\xi = \nabla^2 \psi$$

and

$$\frac{\partial u}{\partial z} = -\frac{g}{f}\frac{\partial}{\partial y}(\Delta s)$$

$$\frac{\partial v}{\partial z} = \frac{g}{f}\frac{\partial}{\partial x}(\Delta s)$$

(In terms of pressure, it can be shown that $\psi \propto \Delta p$).

With a solution of the form.

$$\psi = F(z)\exp(ily)\exp[ik(x-ct)] \quad .. \quad (2.6)$$

representing a wave moving in the x-direction with phase speed C_1 ($C = C_1 + iC_2$), Eady showed that only waves with wavelengths λ satisfying

$$\lambda \geq \frac{\pi H}{f}\sqrt{gB} \quad .. \quad (2.7)$$

can amplify. H is the scale height ($\sim$10Km). Thus λ increases with static stability. For typical values of B and f, the lower cut-off wavelength λ_c = 4000Km, with an e-folding time of about 2 days. In such waves, the trough axis tilts westwards with height.

The characteristics of the cyclones waves of the middle latitudes are very much similar to those of the theory.

ChanneY's theory provided the upper cut-off wavelength and thus completed the fundamental theory of baroclinic instability (See also Holton, J.R. (1972) for a 2-level quasi-geostrophic treatment)

In baroclinic instability, the waves basic amplify because the potential energy of the basic flow is converted into perturbation potential energy which is then converted into eddy Kinetic energy.

2.2 Barotropic Instability

A barotropic atmosphere is one in which there is no vertical shear of the wind - thermal wind is zero. Unlike the mid-latitudes where strong latitudinal temperature gradients provide the primary energy source for synoptic scale disturbances, temperature gradients in tropical regions are small, leading to small available potential energy storage. Energy for disturbances thus comes primarily from latent heat release.

17

Since most tropical disturbances develop in situ, their development cannot usually be accounted for by baroclinic instability.

It is now established that barotropic instability and conditional Instability of the Second Kind (CISK) are two main mechanisms for their initiation. The latter is treated in section 2.4

Starting from the barotropic vorticity equation (1.18) and introducing perturbation velocities as for the quasi-geostrophic theory (but here no assumption of geostrophy!) the linearised perturbation stream function equation may be expressed as

$$\left(\frac{\partial}{\partial t} + \bar{u}\frac{\partial}{\partial x}\right)\nabla^2\psi + \left(\beta - \frac{d^2\bar{u}}{dy^2}\right)\frac{\partial\psi}{\partial x} = 0 \quad . \quad (2.8)$$

Kuo (1949) showed that barotropic instability of the zonal flow is possible if

$$\beta - \frac{d^2\bar{u}}{dy^2} = \frac{d}{dy}(\zeta + f) = 0 \text{ somewhere} \quad .. \quad (2.9)$$

That is, the profile of absolute vorticity must change sign somewhere within the domain of interest (a full treatment of this is in Holton, J.R. (1972) p. 290). Such profiles, taken from Resnick (1976), are shown in Figure 3 which shows that the condition for instability is met only in the month of August at 700mb at longitude 5°E.

Resnick has shown, however, that tropical zonal flows do satisfy the conditions for both barotropic and baroclinic instabilities. That is, that even though horizontal temperature gradients may be small, they are nevertheless sufficient to give some vertical shear of the wind in addition to lateral wind shear.

That this is so was shown by Charney (1973) using the internal jet theory of Charney and Stern (1962). The condition here is that the gradient of potential vorticity $\bar{q}$ must be negative somewhere in the domain:

$$\frac{\partial\bar{q}}{\partial y} = \frac{\partial}{\partial y}(\zeta + f) + \frac{\partial}{\partial p}\left(\frac{p f_0^2}{R\sigma}\frac{\partial\bar{u}}{\partial p}\right) \quad . . \quad (2.10)$$

18

where f_0 is the Coriolis parameter at the centre of the region and σ is static stability defined by $\sigma = T\partial\bar{\theta}/\bar{\theta}\partial p$

The resulting field of $\partial\bar{q}/\partial y$ at 700mb is shown in Figure 4, giving firm indication that both types of instability are important but that the baroclinic terms makes a smaller contribution.

2.3 Convective Instability

Embedded within the synoptic scale systems are mesoscale convective circulations whose initiation and evolution are determined by the stability control of the larger-scale flow and the release of latent heat. In an unsaturated atmosphere, static instability occurs only when, for the lapse rate γ given by

$$\gamma = \Gamma_d - \frac{T}{\bar{\theta}}\frac{\partial\bar{\theta}}{\partial z}, \quad .. \quad (2.11)$$

$$\partial\bar{\theta}/\partial z < 0$$

However, continuous parcel ascent will lead to condensation and latent heat release. Instability continues in this saturated situation if the lapse rate γ is greater than the saturated adiabatic lapse rate Γ_s. The stability condition for such a moist atmosphere is then known as Conditional Instability (i.e. $\Gamma_d > \gamma > \Gamma_s$). This is more conveniently represented in terms of the equivalent potential temperature θ_e which is the temperature an air parcel would have if all its moisture were condensed out and then brought dry adiabatically down to 1000mb level. The process is irreversible. θ_e is given by

$$\theta_e = \theta \exp(Lq_s/c_p T)$$

Thus conditional instability occurs if

$$\partial\theta_e/\partial z < 0$$

It is stable (absolutely) otherwise. This is also known as convective instability. Figure 5 shows that the tropical atmosphere is conditionally unstable in the lower troposphere. However, the release of instability additionally requires low-level convergence to ensure (forced) lifting to saturation. This is because only air below about 900mb has sufficiently high θ_e to become convectively buoyant when forced to rise; much more forced ascent is required for higher layers due to the low θ_e.

2.4 Convective Instability of the Second Kind (CISK)

In the previous two subsections, it was emphasised that, unlike for the mid-latitude synoptic scale systems, latent heat is the major energy source for many tropical circulations. The convective systems are embedded in and controlled by the larger-scale flow.

In this type of arrangement, strong interactions exist the smaller and the larger circulations.

Charney and Eliasen (1964) had shown that ordinary conditional (or convective) instability produces significant growth rate only on the scale of individual cumulus clouds. This is especially so for reasons given in the previous section. The convergence required is on a larger scale and is frictionally driven. With considerable ascent thus ensured, attainment of buoyancy by the rising air parcel is possible and the condensing cloud air then supplies (latent) heat to the larger-scale flow. The interaction is thus co-operative: the larger scale motion supplies needed moisture for cumulus growth through frictional convergence while the cumulus clouds in turn supply the latent heat required to drive the large scale circulation.

When such co-operative interaction leads to th e unstable growth of the larger-scale system, the process is referred to as Conditional Instability of the Second Kind (CISK).

3. RAIN-PRODUCING SYSTEMS OF SEMI-ARID TROPICS

The weather and climate of the tropics and subtropics are influenced mainly by the trades of both hemispheres - the north-east and south-east trades. The latter changes direction on crossing the equartor to become southwesterly flow, popularly known as the southwest monsoon. The marked contrast between the airmass properties (direction and moisture) gives rise to a kind of pseudo-frontal zone - the Inter-Tropical Convergence Zone, ITCZ - where the two trades meet. In West Africa, the continental manisfestation of the ITCZ is called the Inter Tropical Discontinuity, ITD.

It is the seasonal and daily meridional oscillations of the ITCZ or ITD that essentially determine the weather and rainfall patterns of the semi-arid and disturbed areas of the tropics. The location of this zone is shown in Figure 6 for both summer and winter months. A mechanism of ITCZ formation and maintenance was put forward by Charney (1957). Since the low-level tropical air is highly moisture-ladden and is convectively unstable (section 2.3), cumulus convection and latent heat release depend largely on frictional pumping of mass and moisture out of the layer. These are proportional to the vorticity of the surface wind and may be expressed simply as

$$\omega_o = A \zeta_o \qquad .. \quad (3.1)$$

where A depends on the Kinematic coefficient of eddy viscosity (K_m) and the cross-isobaric angle (α) of the winds. Thus in a tropical atmosphere with positive vorticity imparted by a disturbance, frictional convergence will lead to upward pumping of moist air and cloud formation.

The clouds in turn generate condensational warming, fall of pressure and further intensification of the cyclonic vorticity and hence convergence, leading to a perpertuation of the system. This is the CISK process discussed in section (2.4).

However, some of the characteristics of the ITCZ differ significantly from those of the ITD. While weather and precipitation occur in the immediate vicinity of the former, significant weather is not encountered for about 150km south of the surface ITD (Hamilton & Archbold, 1945; Adejokun 1966). Associated with the surface convergences are low-pressure systems whose intensity usually increases with height before weakening. Also, much of the tropical rainfall is from convective clouds (see e.g. Glatnz, 1976; and Omotosho, 1984 for the West African case) of varying dimensions and intensities and are known to be associated with the synoptic-scale pressure disturbances and the monsoons.

In order to get full appreciation of the development and evolution of each of the rain-producing systems and their relative contribution to the precipitation of the semi-arid regions, each system will be treated separately. This is because the semi-arid zones, especially the continental areas, receive meagre but vital precipitation when the appropriate flow region around the ITCZ or ITD reaches and emcompasses the zone. It is also important to note that the meridional oscillation of the ITCZ or ITD is itself dependent on the seasonal variations of the subtropical anticyclonic centres; the failure of these centres to shift appreciably northwards have often led to disastrous rainfall deficits in the semi-arid regions of West Africa

Thus, we shall discuss the following groups of rain-produding tropical circulations:

(a) meso-scale convective systems (cumulus clouds including thunderstorms, squall lines, cloud clusters etc);

(b) synoptic-scale wave disturbances (easterly waves);

(c) Tropical Cyclones and Monsoon depressions;

3.1 The Easterly Waves

Easterly waves are the best known tropical weather systems. First comprehensively studied and documented over the Caribbean by Riehl (1954), it is believed that many of the smaller scale motions (thunderstorms and squall lines) are associated with them.

The characteristics and structures of easterly waves are not the same everywhere round the world, even though attempt had been made to apply the same concepts to waves everywhere. The important differences will be brought out clearly here.

(a) Waves in the Caribbean and Pacific

The model of waves in the easterlies as presented by Riehl is shown in Figure 7.

The westward propagation speed of the waves is 5-7m/s. The wave is weakest at sea-level and increases in intensity upwards to about 600mb (4km) before weakening upwards thereafter. The trade wind inversion is most pronounced about 300 km ahead of the wave through leading to intense subsidence and fine weather. The depth of the moist layer increases rapidly to a maximum at a wave axis.

The Kinematical aspects of easterly waves may be explained from the simplified vorticity equation

$$\frac{d}{dt}(\zeta + f) = -(\zeta + f)\nabla \cdot \underline{V} \quad \ldots (3.2)$$

Since air flows westwards through the wave in the lower layers, the equation implies low-level convergence behind and divergence ahead of the wave axis. The reverse takes place at upper levels where the basic easterlies are weaker and the wave propagates westwards relative to the flow. Thus the area of active and deep convection and heavy precipitation lies to the rear of the trough.

This model appears to have been applied successfully to the West Pacific waves.

(b) African Easterly Waves

Reihl's model cannot be applied piece-meal to the easterly waves over West Africa and the eastern Atlantic. This is because the wind regimes of the areas differ significantly (compare Figure 8a, b and c for Venezuela, West Pacific and West African regions). The juxtaposition of two tropospheric jets over a rather shallow layer of very moist and warm southerly air is unique and are important over West Africa and the eastern Atlantic. Hence the African Zone of wave activity is unusual when compared to the lower troposphere of the rest of the tropics because temperature changes of 10°C can occur within a latitude band of only 10°; the resulting vertical wind shear leads to the mid-tropospheric African easterly jet (AEJ).

The easterly waves develop south of the jet (AEJ) core in a region where the mean zonal flow is barotropically unstable (Burpee, 1972). Wave structure (Figure 9) shows a surface convergence zone only, a cyclonic vortex at 850mb and a distinct wave pattern at 700mb. Wave intensity decreases upwards thereafter. The instability of the flow has been tested from Charney's (1973) extension of the theory of Charney & Stern (1962) for baroclinic instability. This requires a turning point in the meridional gradient of mean potential vorticity ($\bar{q}$) which is represented by

$$\frac{\partial \bar{q}}{\partial y} = \frac{\partial}{\partial y}(\bar{\zeta} + f) + \frac{\partial}{\partial p}\left(\frac{p f_o^2}{R\sigma}\frac{\partial \bar{u}}{\partial p}\right) \qquad .. \quad (3.3)$$

where

$$\sigma = \frac{\bar{T}}{\bar{\theta}}\frac{\partial}{\partial p}\ln\bar{\theta}$$

Charney showed that if surface temperature increases northwards, as is the case in northern Africa, then for instability to occur, $\partial\bar{q}/\partial y$ must be negative somewhere in the domain. Some results, due to Kesnick (1976) are shown in Figure 4. It is obvious that African waves are due to both barotropic and baroclinic instabilities, with the former being the main contributor.

Figure 10 b & c are the vertical profiles of vorticity and divergence in a West Pacific and an East Atlantic wave while Figure 11 shows the distributions of moisture, vertical motion and rainfall amounts around eastern Atlantic waves. There is strongest convergence located ahead of the wave trough where cyclonic vorticity is also strongest. Weather and precipitation distributions are therefore a reverse of the caribbean situation.

Reed (1984) has suggested from use of spectral analysis of data over East Africa, that another type of rain-bearing wave phenomenon found not at the mid-tropospheric levels as in West and Central Africa, exists over the east African region. This wave is however not necessarily different from that over central and west Africa.

3.2 Squall Lines & Thunderstorm

Outside the mid-latitudes, squall lines are generally defined as a belt of intense thunderstorms of 100-300 Km long, 50-100km wide, orientated roughly north-south and moving westwards at about 15m/s on average. They are most common in West Africa, Caribbeans and Venezuelan regions. Together with thunderstorms, they produce more than 80% of total rainfall of the affected areas (see for example Figure 12a from Omotosho, 1985). Many of these meso-scale convective systems are widely believed to be a result of the low-level convergence associated with the synoptic-scale easterly waves where the atmosphere is convectively or potentially unstable. Figure 12b shows that they are found almost anywhere along the wave but mostly ahead of the wave trough. They are therefore not initiated by wave activity (Kebride and Gray, 1980). Some are also associated with asymptotes of convergence in the low-level streamline pattern (Houze 1977) and are then referred to as Disturbance Line.

While the mechanism of their propagation and maintenance are now properly understood, that of their initiation is still unclear.

However, Moncrieff & Miller (1976) and Bolton (1984) have shown that the existence of a tropospheric wind maximum with reversed wind shear in the lower levels is important to their development. The systems are in quasi-steady state with the density current (gust front) feeding the cloud cells with warm, moist (high θ_e) air for sustenance (see Figure 13). It is also being suggested that the simultaneous presence of positive boundary layer vertical wind shear, a moist layer of about one kilometre deep and a distinct and organized mid $\longleftarrow\longrightarrow$ tropospheric wind maximum (AEJ) are all necessary conditions for widespread thunderstorms development and their alignment into a line, as shown in Figure 14. The interaction between the clouds, gust front and the boundary layer is essentially one of CISK. Such interaction is possible only because of the peculiar wind regimes which causes the relative flow to enter the storm clouds from the front.

Moncrieff & Miller gave the speed of propagation of tropical squall lines C_s as

$$C_s = U_m + 0.3\sqrt{CAPE} \quad .. \quad (3.4)$$

where U_m is the mid-level wind speed in the cumulonimbus layer, CAPE is the convective available potential energy which is proportional to the positive area on the T-ϕ gram. Equation (3.4) was found to give speeds C_s in considerable agreement with observation for squall lines over Venezuela (Betts et al, 1976) and reasonably so over west Africa (Omotosho, 1976) but as pointed out by Omotosho (1984), evaluation of CAPE is not practically convenient for operational purposes. He suggested a predictive relation (from actual data and based on similar interaction principle) of the form,

$$C_s = aU_m + b\Delta T \quad .. \quad (3.5)$$

where $$\Delta T = \left[(T_{S2} - T_M)/T_{S2}\right]^{1/2}$$

T_{S2} is the surface temperature two hours before squall arrival, a & b are constants determined for individual stations.

The manner in which the interaction is used to the advantage of the squall line is summarised in Figure 13. Cool dry air is sucked from the front into the cloud at the level of the AEJ, rushes down as evaporative downdraft to force the southwest warm moist air up into the clouds at the gust front created as a result of their temperature contrasts. The exact role of the upper tropical easterly jet (TEJ) is however not yet clear.

3.3 Monsoon Depressions

Monsoons are caused by the different response of land and ocean to solar radiation, confined largely to the tropics and are periods of concentrated precipitation.

Over large tropical oceans, seasonal changes in circulations are limited to minor latitudinal shifts of the winds and cloud distributions, with the general pattern remaining virtually the same all year round. An entirely different situation exists over tropical continents and adjacent oceans where large seasonal temperature variations occur. The consequence is that the regions of the semi-permanent anticyclones over the oceans, and which extend over the land areas of the tropics in winter, are quickly transformed at the beginning of the summer into areas of low pressure over the continents, leading to the establishment of the ITCZ (or ITD) some distance from its winter position.

The trade (S.E) winds of the southern hemisphere cross the equator, change direction due to the reversal of the Coriolis force and become south-westerlies. This means that tropical continents and adjacent oceans experience a semi-annual wind reversal known as the monsoons.

The monsoon, especially the summer type, therefore represents large-scale air flow from the oceans to the tropical regions of the Middle East, particularly India, Southern Asia and West Africa. The areas of monsoon circulations are depicted in Figure 15. The winter monsoon over India and Southern Asia is a period of 'short' rain whereas it is entirely a dry period over West Africa. In contrast, the summer monsoon is a time of widespread and prolong precipitation everywhere affected by the monsoon. This is because large-scale flows with strong westerly components are associated with vertically increasing Kinetic energy of the perturbation upward motion (Jeffreys, 1956) as

$$\frac{\partial}{\partial z}(w'^2) = 2\Omega u \cos\phi \qquad .. \quad (3.6)$$

where w' is the perturbation vertical velocity and u is the zonal component of the wind.

(a) The Monsoon Depressions of Southern Asia

The major features of the circulation over southern Asia is depicted in Figure 16. At the surface and low levels, the monsoon is characterised by a semi-synoptic scale low pressure (Figure 17) which becomes most intense in the 800-600mb layer (Ramage, 1971). The disturbances last for upto a week, causing widespread rainfall. Most significant is the appearance of the equatorial jet at 150mb which is connected with the formation of an upper level high pressure system over the Tibetan Plateau during the Summer months; the southwest monsoon is very active during this period. The retreat of the monsoon from over northern India is indicated by the weakening and disappearance of the easterly jet over Western India Ocean.

The strong low-level convergence combined with the active divergence in the upper-level easterlies, leads to strong upward motion which is intensified by the large latent heat release.

The associated precipitation is heaviest over the hatched area in Figure 17.

(b) The West African Monsoon

The West African monsoon occurs on a relatively smaller scale. The seasonal shift of the low-pressure centre (ITD) is only about 17° latitude compared to about 30° for the Indian monsoon. The depression here is essentially a heat low as the zones of maximum temperatures in both winter and summer are almost coincident with the low pressure areas.

The meridional variation in the depth of the monsoon layer is of great importance to the type and intensity of weather over the region, as the ITD moves from its (lowest) latitude of 6°N in February to about 23°N in August. Hence the regions surrounding and influenced by the ITD were zoned as A, B, C and D (Hamilton & Archbold, 1945), depicted in Figure 18a, relative to the ITD and the depth of the moist layer. Details of the zones and associated weather are given in Figure 18b. It is obvious that the most active weather does not occur where the monsoon flow is deepest — the specific humidity (Figure 19) is maximum along latitude 12°N whereas the moist layer is deepest much further south. The January situation is in complete contrast with no rainfall at all over continental West Africa as the convergence zone is over coastal areas.

The monsoon over West African is believed to have a periodicity of 4-6 days (Adefolalu, 1974). Because of the progressively shallower moist layer depth as one approaches the surface position of the ITD contrasting weather and cloud types with varying rainfall intensity and amount are encountered.

The dynamics of the flow is basically governed by the north-south temperature gradient, which is positive polewards at this time. The implied easterly wind shear therefore leads to the weakening of the monsoon with height and the eventual change into easterlies. The monsoon depth may reach about 3km (700mb) in August, considerably weakening or completely preventing wave and deep convective activity.

As nature's most destructive weather systems, tropical cyclones represent a special class of intense atmospheric vortices. Although there is as yet no universal agreement about the processes which lead to the transformation from tropical disturbances to cyclones, Gray and his group at Colorado State University (Gray 1979, Mcbride 1979) have carried out extensive observational studies on the systems. They suggest that tropical cyclones develop in regions where

(a) there is a non-zero value of the Coriolis parameter

(b) the sea surface temperature $> 26.5^{o}C$

(c) there is higher than normal relative humidity

(d) there is zero or negligible vertical wind shear near the centre of the system

(e) a weak warm-core system with a low-level cyclonic circulation having a high value of relative vorticity on the scale of about 500-800km exists and the vorticity falls off with height.

The temperature constraint is necessary to maintain a saturated adiabatic lapse-rate throughout the troposphere with a tropopause temperature of -78°C (Pearce, 1981).

The origins and areas affected by cyclones are depicted in Figure 20a while Figure 20b shows the latitudes of their initial detection. The latter figure shows that cyclones do not form 4-5° from the equator, are most favoured in the latitude belt 5-20°, and are most frequent in the North West Pacific.

In a tropical cyclone, the balance of forces is between the centrigugal force of winds rotating at speeds greater than about 50m/s and the pressure gradient force over a horizontal scale of about 100km. Motion is in hydrostatic balance and there are large temperature deviations.

A tropical cyclone has a well-defined central region - the eye - whose formation depends on the angular momentum of an annular ring of rotating air as

$$V_\theta r = \text{constant} \qquad .. \quad (3.7)$$

where V_θ is the tangential velocity and r the radial distance from the centre. As the centre of the storm is approached (r decreases) the tangential velocity increases. But since the cyclone kinetic energy is finite, the wind cannot increase indefinitely and it thus tends to spiral upwards round a central region of calm subsiding motion.
Figure 21 is a typical vertical cross-section accross a tropical cyclone. The eye is warmer than its environment throughout its depth, making tropical cyclones warm-core systems.

Cyclone genesis would seem to depend on the strength of low-level cyclonic and upper tropospheric anticyclonic circulations. Their genesis may be thought of from the conditions which lead to an increase in the absolute angular momentum, M_a, within a cylindrical area of the disturbance region out to about 6° radius.
This can be represented by

$$\int \frac{\partial m_a}{\partial t} \delta M = -\int_{100}^{p_s} \int_0^{2\pi} \frac{V_r m_a}{g} \delta\theta \delta p + \int r F_\theta \delta M \qquad (3.8)$$

where $m_a = V_\theta r + \frac{1}{2} f r^2$

and $$\int \delta M = \int_{100}^{p_s} \int_0^{2\pi} \int_0^{6^\circ} \frac{r}{g} \delta r \delta\theta \delta p$$

V_r, V_θ, p_s represent radial tangential winds and surface pressure respectively.

The term of LHS is the mean rate of change in momentum within the disturbance. The first term on the right represents the import of momentum at the 6° radius boundary into the region; the last term is the momentum dissipation. Observational results have indicated that there is a much

value of second over last term in (3.8)

The difference between the relative vorticity at lower and upper troposphere, the so-called 'genesis potential', is also an important factor. Developing cyclones are found to be characterised by large differences

This difference is concentrated in the lower and upper troposphere as shown in Figure 22.

Cyclone intensification have mostly been modelled on the CISK theory. While the theory appears to give satisfactory explanation of the later stage and inner-core region intensification, it does not explain how the deep cyclone from which integrations started is itself formed.

Much further modelling assisted by results from observational study are still required before cyclone understanding and prediction can be fully achieved.

4. BOUNDARY PROCESSES AND SURFACE ENERGY BUDGET

In section 1.4, the radiative processes and energy balance were discussed. This balance may be expressed as

$$Q = Q_H + Q_E + Q_G \quad . \quad . \quad (4.1)$$

where Q_H and Q_E are the sensible and latent heat fluxes out of the surface and Q_G the flux into the ground. Q (the basic input of surface energy budget) is the net radiation absorbed by the ground as a consequence of which its temperature changes according to time of the day (see Figure 23) When energy storage, ΔQ_S, in the layer (or slume) is considered, (4.1) becomes

$$Q = Q_H + Q_E + Q_G + \Delta Q_S \quad . \quad (4.2)$$

These equations express the concept

Energy Input - Energy output - Storage = 0

Three possibilities exist:

(a) Input > Output $\Rightarrow$ flux convergence (ΔQ_S 0)

(b) Input < Output $\Rightarrow$ flux divergence ($\Delta Q_S < 0$)

(c) Input = Output ($\Delta Q_S = 0$).

The temperature of a layer of air near the ground can be changed by the convergence or divergence of one or more of Q, Q_H, Q_E and Q_A (horizontal flux). If the site is assumed free of horizontal advection and the air remains unsaturated, then only Q and Q_H effect the change in the air temperature. Hence the atmosphere is warmed by day when Q_H is directed upwards and vertical turbulence mixing is efficient with Q remaining effectively constant with height. The night situation is that Q_H is directed into the ground and the air is cooled by the vertical divergence of Q_H ($-\Delta Q_H$). Upto about 50m above the ground variations in radiatively-important agents (water vapour, CO_2, dust) is negligible; this is the constant-flux layer.

The rate of heat flow into and out of the soil depends on the temperature gradient and the soil characteristics, so that the flux-gradient relationship is

$$Q_G = -k_s \frac{\partial \bar{T}}{\partial z} \quad . \quad . \quad (4.3)$$

where k_s is the thermal conductivity ($W m^{-1} K^{-1}$); it is not strictly a constant as it varies with depth and time. Thus by day time when $\partial \bar{T}/\partial z$ is negative, Q_G is positive into the air (i.e. a surface energy loss). The general diurnal and seasonal cycles of soil temperature at different depths are shown in Figure 24a and b while Figure 24c is for a tropical continental station (Ile-Ife, Nigeria). The heat wave penetrates to lower depths with decreasing amplitudes and the maximum and minimum temperatures are time-lagged. Both features are dependent on the thermal diffusivity k_s ($= k_s/C_s$, C_s is the thermal capacity)

The wave amplitude at any depth $(\Delta T_s)_z$ decreases exponentially with time as

$$(\Delta T_s)_z = (\Delta T \exp\left[-z\left(\pi/k_s P\right)\right] \quad . \quad . \quad (4.4)$$

where P is the wave period.

The method of estimating heat flux Q_G is to use heat flux plate of known conductivity since the variability of k_s renders equation (4.3) impracticable. The plates are usually buried horizontally and at least 10mm below the soil surface. The temperature gradient across, and the heat flux through, the plate (and hence the soil) are proportional to the output of the plate as measured by the connected thermopile. Due to the plate's closeness to the surface, over - (or under-) estimation may occur. This is accounted for by subtracting (adding) the change in heat storage (ΔQ_s) in the overlying layer.

A similar equation to (4.3) is also valid for the flow of water, M_v from the soil:

$$M_v = -\rho k_w \frac{\partial \bar{q}}{\partial z} \quad . \quad . \quad (4.5)$$

where ρ is air density, k_w the molecular diffusivity for water vapour ($\approx 0.20 \times 10^{-4} m^2 s^{-1}$) and q is the specific humidity.

Equations (4.3) and (4.5) are strictly valid in the soil or laminar boundary layer but not in the atmosphere where convective activity dominates and real molecular transfer is negligible. Despite this, the analogy of the roles of molecules in conduction can be extended to that played by eddies in convection. The transfer of horizontal momentum in the laminar boundary layer is given by

$$\tau = \rho k_m \frac{\partial \bar{u}}{\partial z} \quad . \quad . \quad (4.6)$$

where τ is the shearing stress (force per unit area) to the kinematic viscosity ($\simeq 0.15 \times 10^{-4} m^2 s^{-1}$), $\bar{u}$ the mean wind. The analog for the turbulent surface layer above this laminar layer is

$$\tau' = \rho K_m \frac{\partial \bar{u}}{\partial z} \quad . \quad . \quad (4.7)$$

where Km is the eddy viscosity ($m^2 s^{-1}$). Km is about 5 orders of magnitude greater than k_m.

The study of momentum exchange is important because it is central to studies concerning transports of heat (Q_H) and moisture (Q_E) and also to pollutant dispersal.

Under conditions of neutral stability, the variation of wind with height is given by the logarithmic wind profile equation:

$$\bar{u} = \frac{u_*}{k} \ln\left(z/z_o\right) \quad . \quad . \quad (4.8)$$

where $\bar{u}$ is the wind speed at height z, u_* ($u_*^2 = \tau/\rho$) is the friction velocity, k the von Karman's constant (0.40), and z_o is the roughness length (m). Since u_* can be evaluated from wind profile measurements (slope is k/u_* from (4.8)) the stress τ can be obtained which can then be used for evaluating other fluxes.

The above discussion relates to neutral conditions where buoyancy is unimportant, as in cloudy skies and strong winds. In such situations forced convections due to frictionally-generated eddies dominate. In unstable conditions momentum, heat and moisture exchanges are enhanced, although forced convection are still dominant near the ground up to say about 2m. Above this level, free convection becomes dominant and stability effects on vertical exchanges increases, Figure 25 gives the wind profiles under different stability conditions. Vertical wind gradients are largest under stable situations and weakest in an unstable atmosphere.

4.1 Heat and Moisture Fluxes

The sensible heat Q_H passing through the laminar boundary layer by molecular conduction is

$$Q_H = -\rho c_p k_H \frac{\partial \bar{T}}{\partial z} \quad . \quad . \quad (4.9)$$

and the flux of sensible heat in the overlying turbulent layer is given by

$$Q'_H = -\rho c_p K_H \left(\frac{\partial \bar{T}}{\partial z} - \Gamma_d \right) \quad . \quad (4.10)$$

or, in terms of potential temperature θ

$$Q'_H = -\rho c_p K_H \frac{\partial \bar{\theta}}{\partial z} \quad . \quad . \quad (4.11)$$

K_H is the eddy heat conductivity ($m^2 s^{-1}$). The vertical transport of sensible heat is typicalised in Figure 4.26 which shows the correlation between stability, temperature and the heat flux. Large upward heat transfer and high temperature are associated with unstable conditions (w positive).

Evaporation from the surface through the laminar sub-layer is given by equation (4.5). The flux of the water vapour in the turbulent layer is

$$E = -\rho K_W \frac{\partial \bar{q}}{\partial z} \quad . \quad . \quad (4.12)$$

and the latent heat flux Q_E is

$$Q_E = -\rho L K_W \frac{\partial \bar{q}}{\partial z} \quad . \quad . \quad (4.13)$$

where K_W is eddy diffusivity and L the latent heat of vaporisation.

The exchange of moisture between surface and the atmosphere determines the humidity. In constrast to the heat flux which is upwards by day and downward towards the surface during the night, water vapour flux is predominantly upwards. Although water may return to the surface as dew under certain conditions, this is almost negligible compared to the daytime flux.

Figure 4.26 shows that the vertical transfer of sensible heat is correlated with the upward motion. The flux of a quantity χ with fluctuations χ' about its mean $\bar{\chi}$ can thus be expressed as

$$F_\chi = \rho \overline{w' \chi'}$$

where the overbar may be time or space average. Therefore sensible and latent heat fluxes may be given as

$$Q_H = \rho c_p \overline{w' T'}$$
$$Q_E = \rho L \overline{w' q'} \quad . \quad . \quad (4.13)$$

However, instrumental response to turbulence is a great problem especially near the ground and this direct method of flux estimation is not widely used. With the present technological advance, there is great hope of applying this simple straightforward technique which is independent of nature of the surface (roughness) and stability.

The profile method which is commonly used is based on the assumption of $K_m = K_h = K_w$. In such cases, the ratios of the fluxes are

$$Q_H / Q_E = \frac{c_p}{L} \frac{\Delta \bar{\theta}}{\Delta \bar{q}} \quad . \quad . \quad (4.14a)$$

$$Q_E / \tau = -L \frac{\Delta \bar{q}}{\Delta \bar{u}} \quad . \quad . \quad . \quad (4.14b)$$

Even if the assumption was not made, a knowledge of the behaviour of, say, K_m / K_H would still allow the above method.

There are two techniques under the profile method - the aerodynamic and Bower ratio methods. The aerodynamic method is strictly valid for neutral conditions only under the assumption of steady-state, invariant fluxes with height and constant Ks.

With these the various fluxes are estimated. With $\partial\bar{u}/\partial z = u_*/k_z$ from (4.8), they are given by:

$$Q_H = -\rho c_p k^2 z^2 \left(\frac{\Delta \bar{u}}{\Delta z} \cdot \frac{\Delta \bar{\theta}}{\Delta z} \right) . \quad (4.15a)$$

$$Q_E = -\rho L k^2 z^2 \left(\frac{\Delta \bar{u}}{\Delta z} \cdot \frac{\Delta \bar{q}}{\Delta z} \right) . \quad (4.15b)$$

The Bowen ratio method has the advantage of being stability-independent . The Bowen ratio β is given by

$$\beta = \frac{Q_H}{Q_E} = \frac{c_p}{L} \cdot \frac{\Delta \bar{\theta}}{\Delta \bar{q}} \quad . \quad (4.16)$$

so that from the surface energy balance equation (4.1), the fluxes can be written in terms of β as

$$Q_H = \beta (Q - Q_a)/(1+\beta) \quad (4.17a)$$

$$Q_E = (Q - Q_a)/(1+\beta) \quad (4.17b)$$

The partitioning of the energy over different surfaces at various locations are shown in Figure 27.

Further discussion of measurements is done under "Satellite Meteorology".

Adefolalu, D.O. 1974: On Scale interaction and lower tropospheric summer easterly perturbation over tropical West Africa. Ph.D. Thesis, Department of Meteorology, Florida State University, U.S.A.

Adejokun, J.A. 1966: The Three dimensional structure of the Inter tropical Discontinuity over Nigeria. Techn. Note No. 39, Nigerian Meteorology Department, Lagos.

Babatunde, E.B. and Balogun, E.E. 1983: The diurnal temperature variation near the ground surface at a tropical station, Nigerian Meteorology Journal, 2, 65-82.

Betts, A.K., Grover, R.W. and Moncrieff, M.W. 1976: Structure and motion of tropical squall lines over Venezuela, Quart J.R. Met. Society, 102, 395-404.

Burpee, R.W. 1972: The origin and structure of easterly waves in the lower troposphere of North Africa. J. Atm. Sci., 29, 77-90.

Charney, J.G. 1947: The dynamics of long waves in a baroclinic westerly current in J. Meteorology, 4, 135-162.

Charney, J.G. and Eliassen, A. 1964: On the growth of the hurricane depression J. Atm. Sci., 21, 159-172.

Charney, J.G. and Stern, M.E. 1962: On the stability of internal baroclinic jets. J. Atm. Sci., 19, 159-172.

Charney, J.G. 1967: The Intertropical Convergence Zone and the Hadley circulation of the atmosphere. WMO/IUGG proceedings on Numerical Weather Prediction Tokyo.

Eady, E.T. 1949: Long waves and cyclone waves. Tellus 1, 33-52.

Glantz, M.H. 1976: Value of a reliable long range climate forecast for the Sahel: A preliminary Assessment. INTAS commissioned study report.

Gray, W.M. 1979: Hurricanes: their formation, structure and likely role in the tropical circulation. In "Meteorology Over Tropical Oceans"

Hamilton, E.A. and Archbold, J.W. 1945: Meteorology of Nigeria and adjacent territory. Quart J. R. met. Soc., 71, 245-262.

Holton, J.R. 1972: An Introduction to dynamic meteorology. Academy Press.

Houze, R.A. 1977: Structure and dynamics of a tropical Squall-line system. Mon. Wea. Rev., 105, 1540-1567.

Leroux, M. 1983: The Climate of Tropical Africa. Editions Champion.

Lettau, H. 1956: Theoretical notes on the dynamics of equatorial atmosphere Beitrage Zur Physik der Atmosphare, 29, 107.

Lockwood, J.G. 1974: World Climatology: An Environmental Approach. Fletcher & Son Ltd., Norwich, Britain.

Lorenz, E.N. 1967: The Nature and theory of the General Circulation of the atmosphere W.M.O. - Nos 218 TP 115, Geneva.

Moncrieff, M.W. and Miller, M.J. 1976: The dynamics and simulation of tropical cumulonimbus and squall lines. Quart. J.R. Met. Soc., 102, 373-394.

[illegible], J.-., 1976: A survey of the tephigram pr and wind fields over tropical West Africa and their relation to the Line Squall. B.Sc Project. Dept. of Met. University of Reading.

[illegible], J. Bayo 1983: Prediction of maximum gusts in West African Line Squalls. Nigerian Met. Journal, 1, 94-100

[illegible], J. Bayo 1984: On the initiation and organisation of deep convective systems over West Africa. Invited Paper. W.M.O conference on Tropical Meteorology in Africa. Dakar, 154-157.

[illegible], J. Bayo, 1985: The separate contributions of line squalls, thunderstorms and the Monsoon to the total rainfall over Nigeria. J. of Climatology (in print).

[illegible], V.P. 1978: On the concept of available potential energy. Quart. J.R. Met. Soc., 104, 737-755.

[illegible], J., Norquist, D.C. and Recker, [illegible] 1977: The structure and properties of African wave disturbances. Mon. Wea. Rev., 105. 317-333.

[illegible], [illegible] 1984: Westward-travelling, synoptic-scale disturbances of the northern hemisphere summer in tropical northern Africa and the adjacent Atlantic. Invited Paper W.M.O. Conference on Tropical Meteorology in Africa. Dakar, 126-133.

[illegible], H. 1954: Tropical Meteorology. McGraw-Hill, New-York.

[illegible], [illegible] 1976 The generation of African Waves. J. Atm. Sci., 33 1955-1969.

Wallace, J.M. and Hobbs 1977: Atmospheric Science: An Introductory Survey, Academic Press New York.

[illegible], R. 1976: Tropical disturbance intensification, Department of Atmos. Sci., Paper No. 249, Colorado State University, Ft. Collins, Colorado.

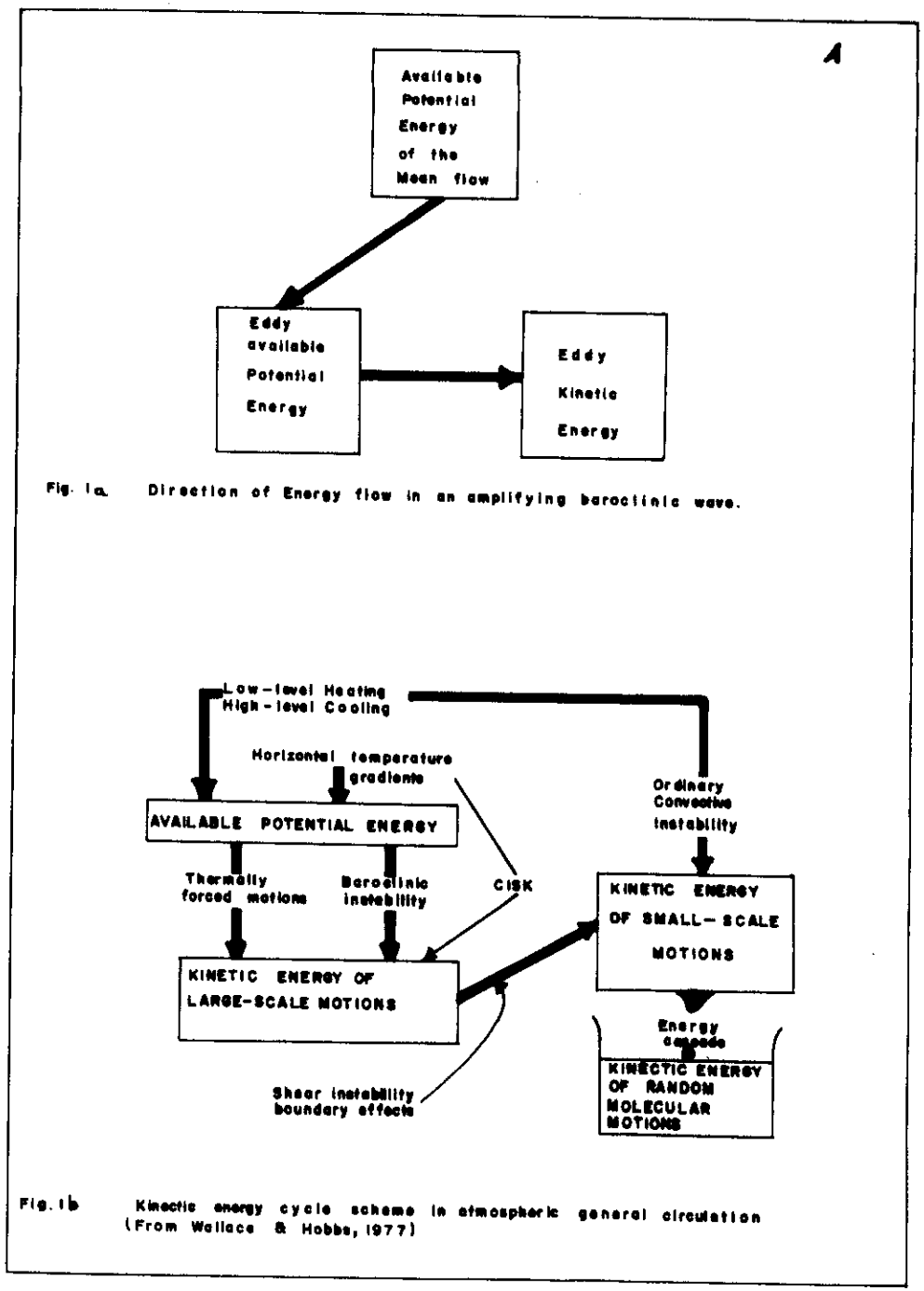

Fig. 1a Direction of Energy flow in an amplifying baroclinic wave.

Fig. 1b Kinetic energy cycle scheme in atmospheric general circulation (From Wallace & Hobbs, 1977)

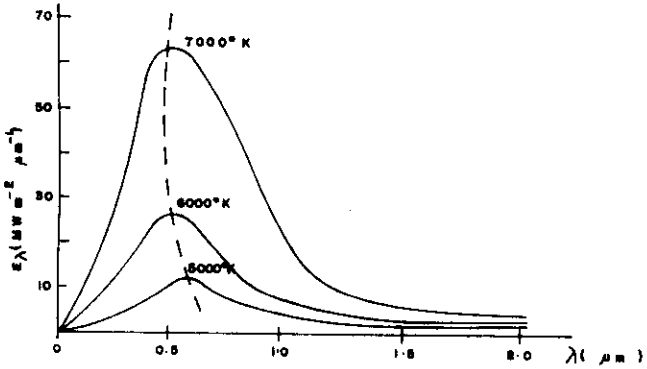

Fig. 2a Black-body emission at indicated temperatures.

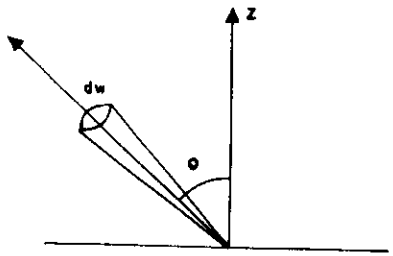

Fig. 2b The solid angle

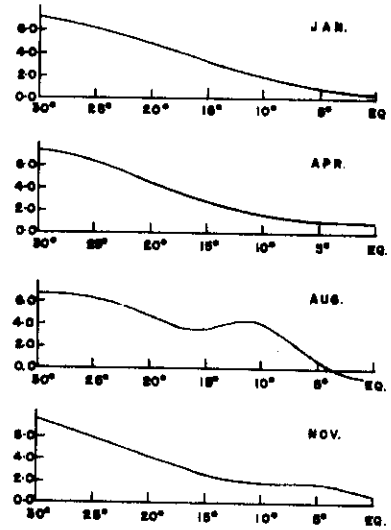

Fig. 3. Absolute vorticity ($\times 10^{-5} s^{-1}$) versus latitude at 5°E, 700 mb

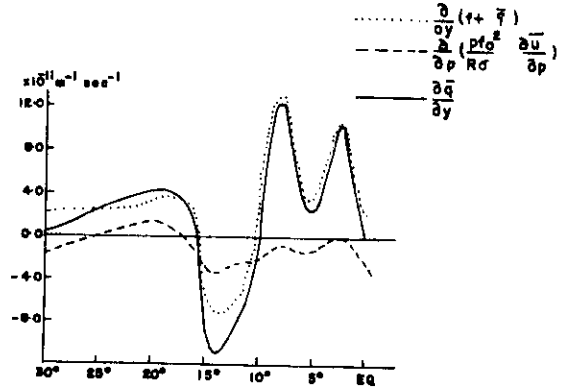

Fig. 4. Gradient of pseudo-potential vorticity versus latitude at 5°E, 700 mb

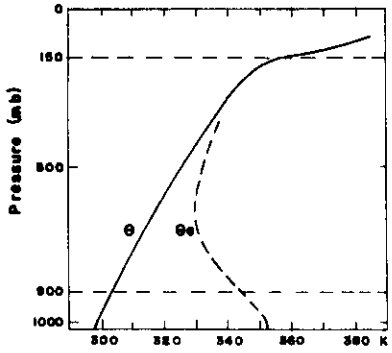

Fig. 5. Typical sounding in the atmosphere showing the vertical profiles of potential temperature θ, equivalent potential temperature θe (adapted from Holton, 1972.)

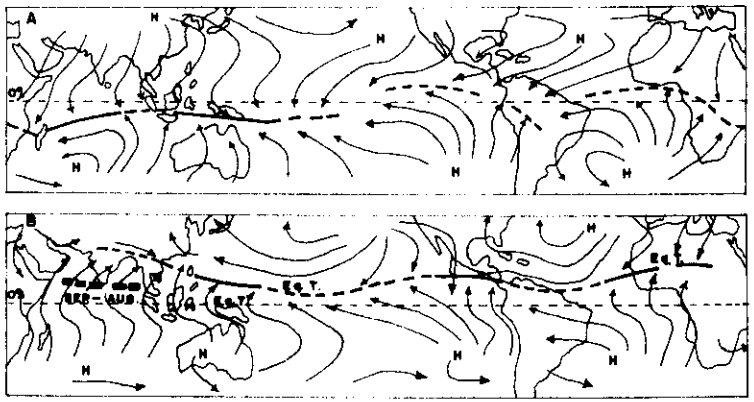

Fig. 6. Idealized surface wind conditions. A : January. B : August. (After Gray, 1968.

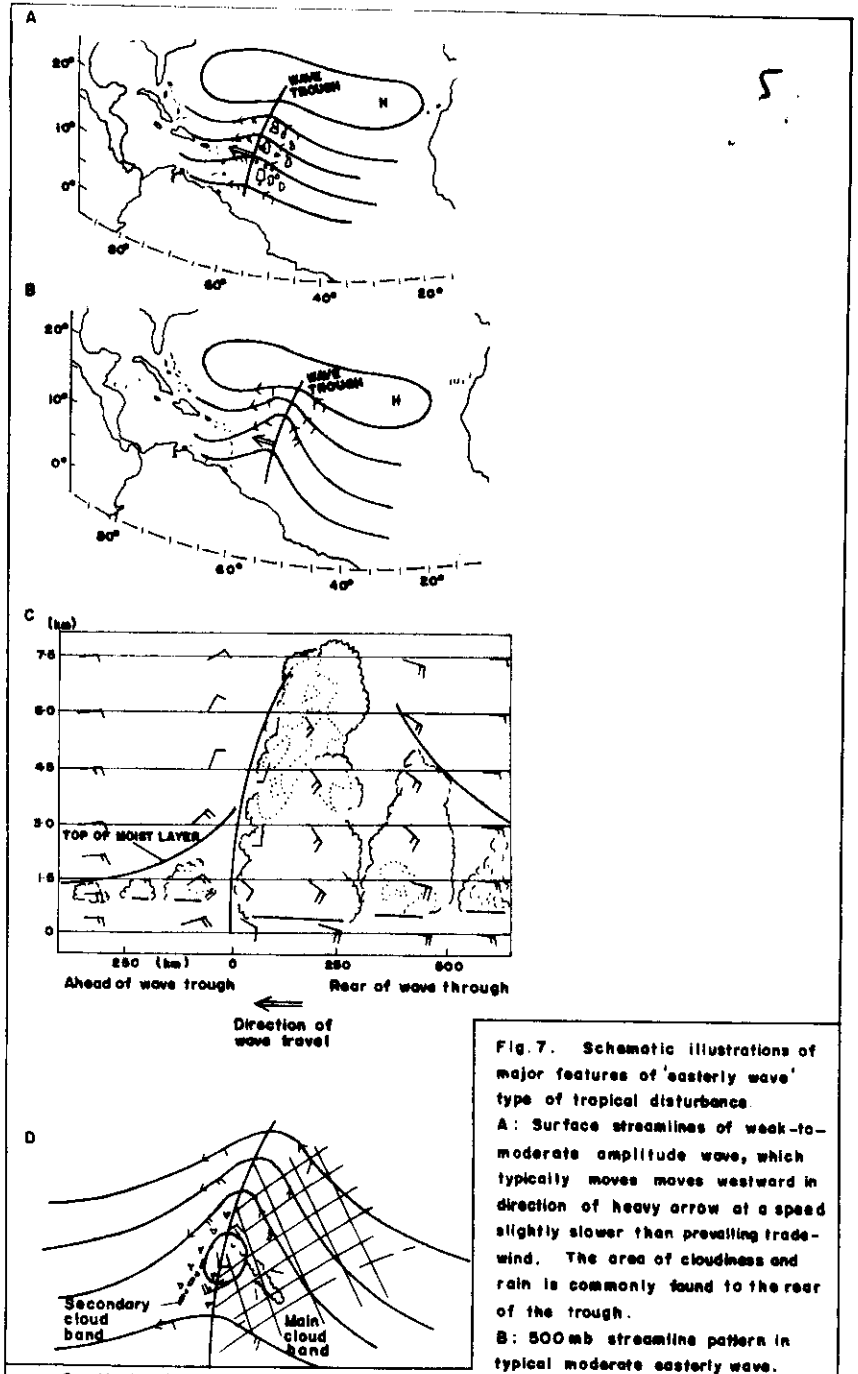

Fig. 7. Schematic illustrations of major features of 'easterly wave' type of tropical disturbance.
A : Surface streamlines of weak-to-moderate amplitude wave, which typically moves moves westward in direction of heavy arrow at a speed slightly slower than prevailing trade-wind. The area of cloudiness and rain is commonly found to the rear of the trough.
B : 500 mb streamline pattern in typical moderate easterly wave.
C : Vertical cross-section from west (left) to east (right). Cloud forms are shown schematically and not to scale.
D : Schematic picture of a very deep easterly wave, showing streamlines and major cloud lands.

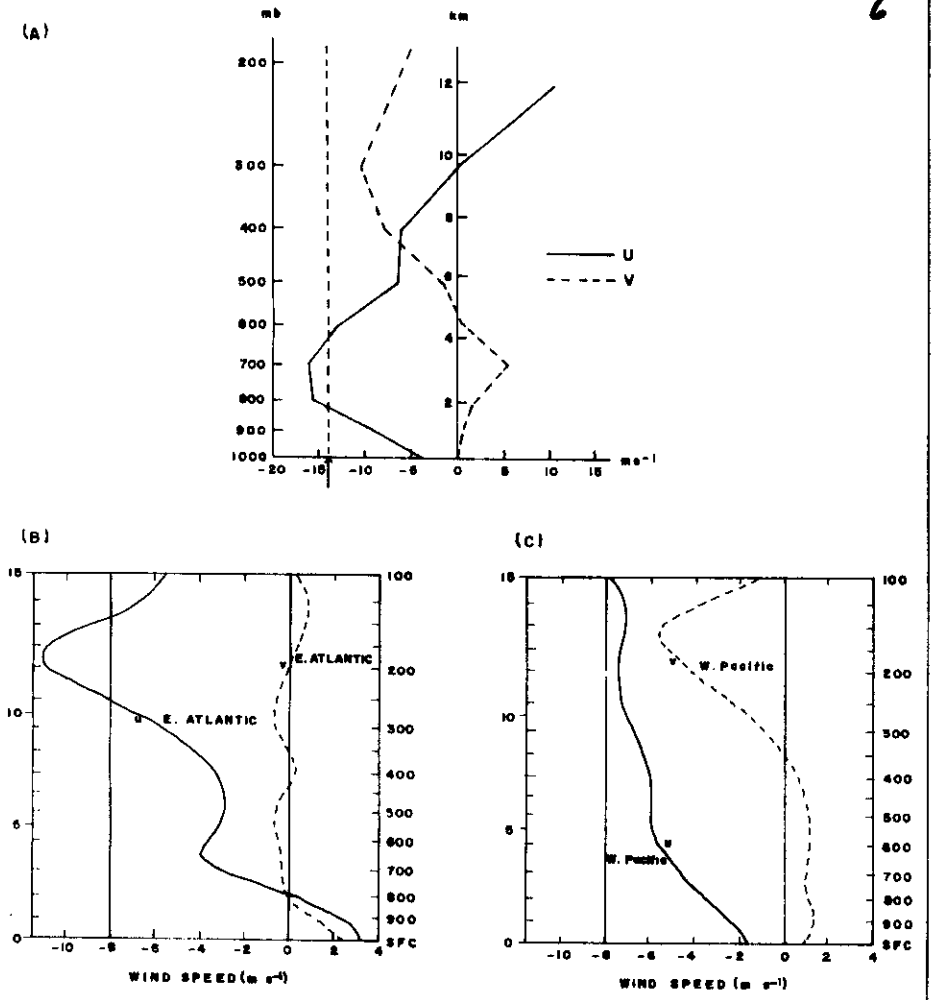

Fig. 8. WIND COMPONENT PROFILES FOR (A) VENEZUELA, (B) WEST AFRICA, AND (C) WEST PACIFIC REGIONS.

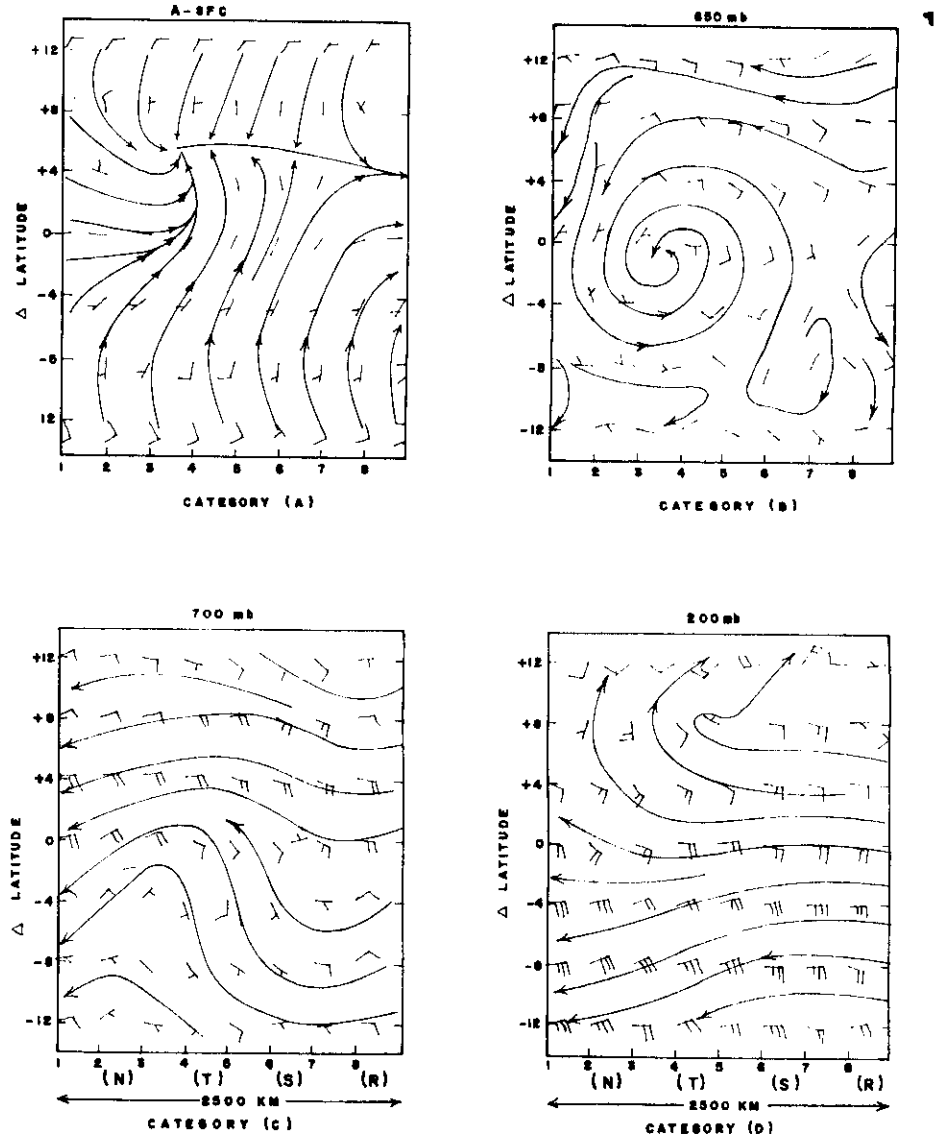

Fig. 9. Streamline analyses of the total wind field associated with the waves at (A) surfa (B) 850mb, (C) 700mb, and (D) 200mb. The plotting convention has been designed so t one half barb equals 2·5 ms⁻¹ and a full barb equals 5 ms⁻¹. The 0 latitude is approximately 11°N (taken from Reed et al, 1977)

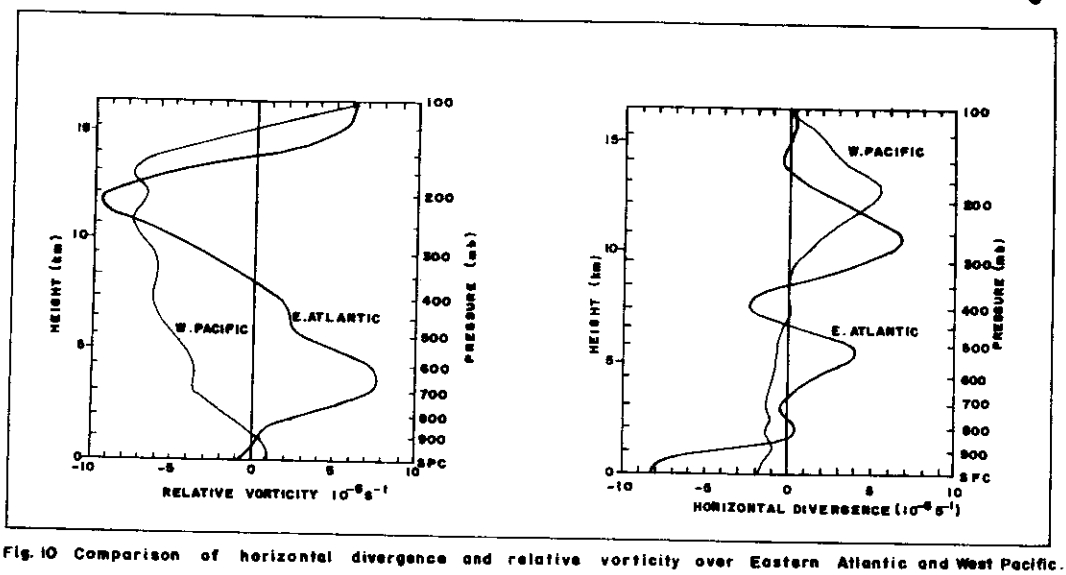

Fig. 10 Comparison of horizontal divergence and relative vorticity over Eastern Atlantic and West Pacific.

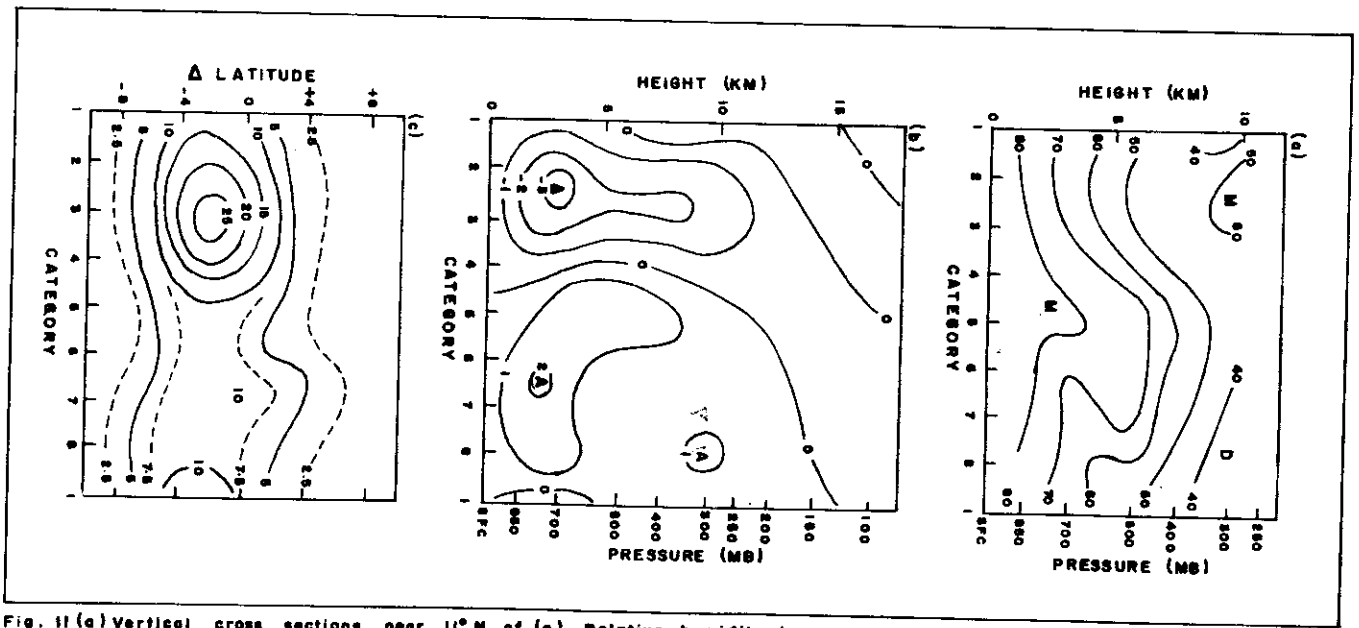

Fig. 11 (a) Vertical cross sections near 11° N of (a) Relative humidity in percent
(b) Vertical velocity in mb h^{-1}
(c) Map of rainfall amounts in mm day (reproduced from Reed et al. [18])

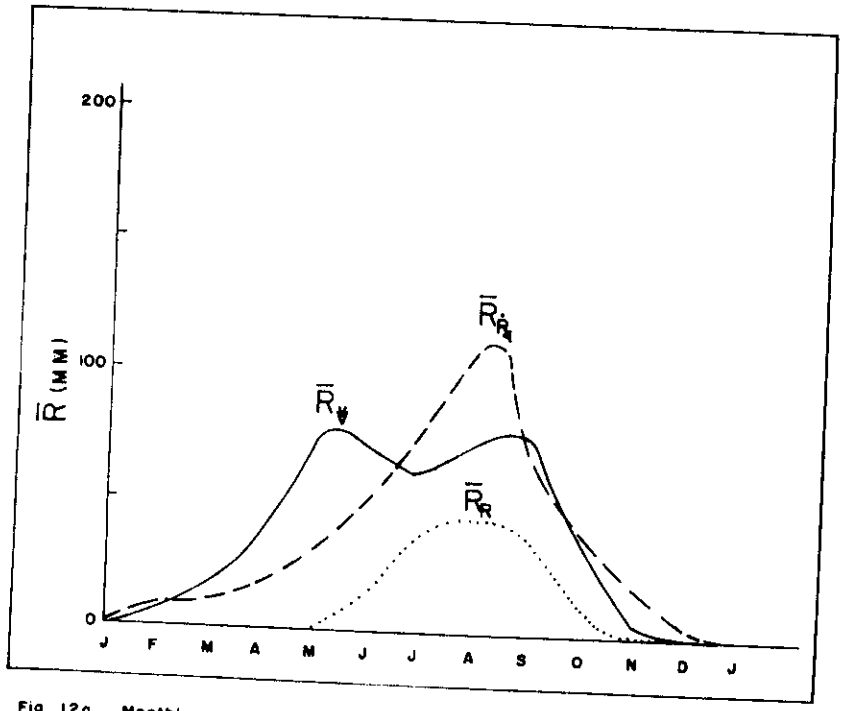

Fig. 12a. Monthly variation of precipitation from line squall..... R_{Ψ}
Thunderstorm ..... $R_{\dot{R}}$
The monsoon ..... R_{R}
(From Omotosho 1985)

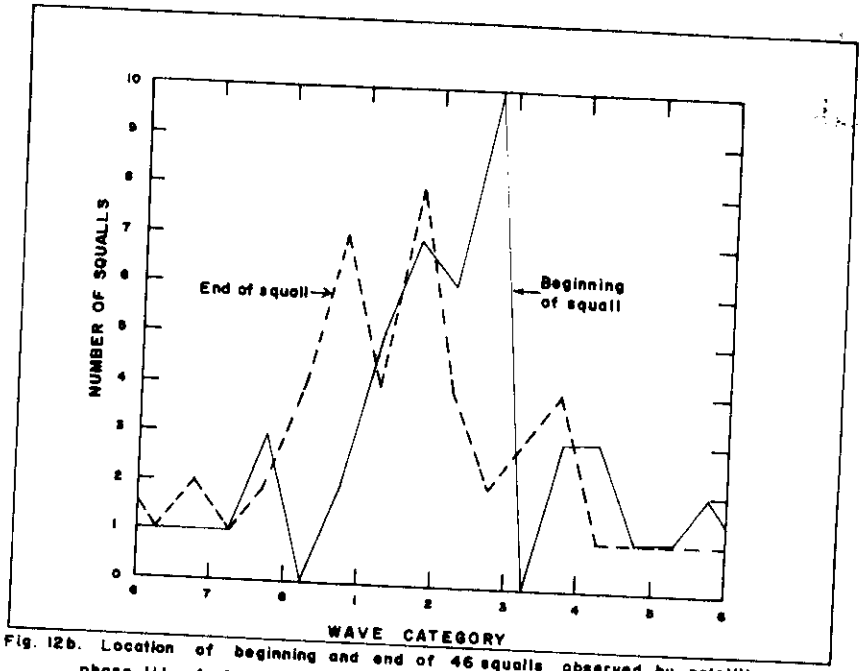

Fig. 12b. Location of beginning and end of 46 squalls observed by satellite during phase III of GATE and the previous interphase period, plotted to the wave category (unpublished diagram; Reed, Payne & McCarty.)

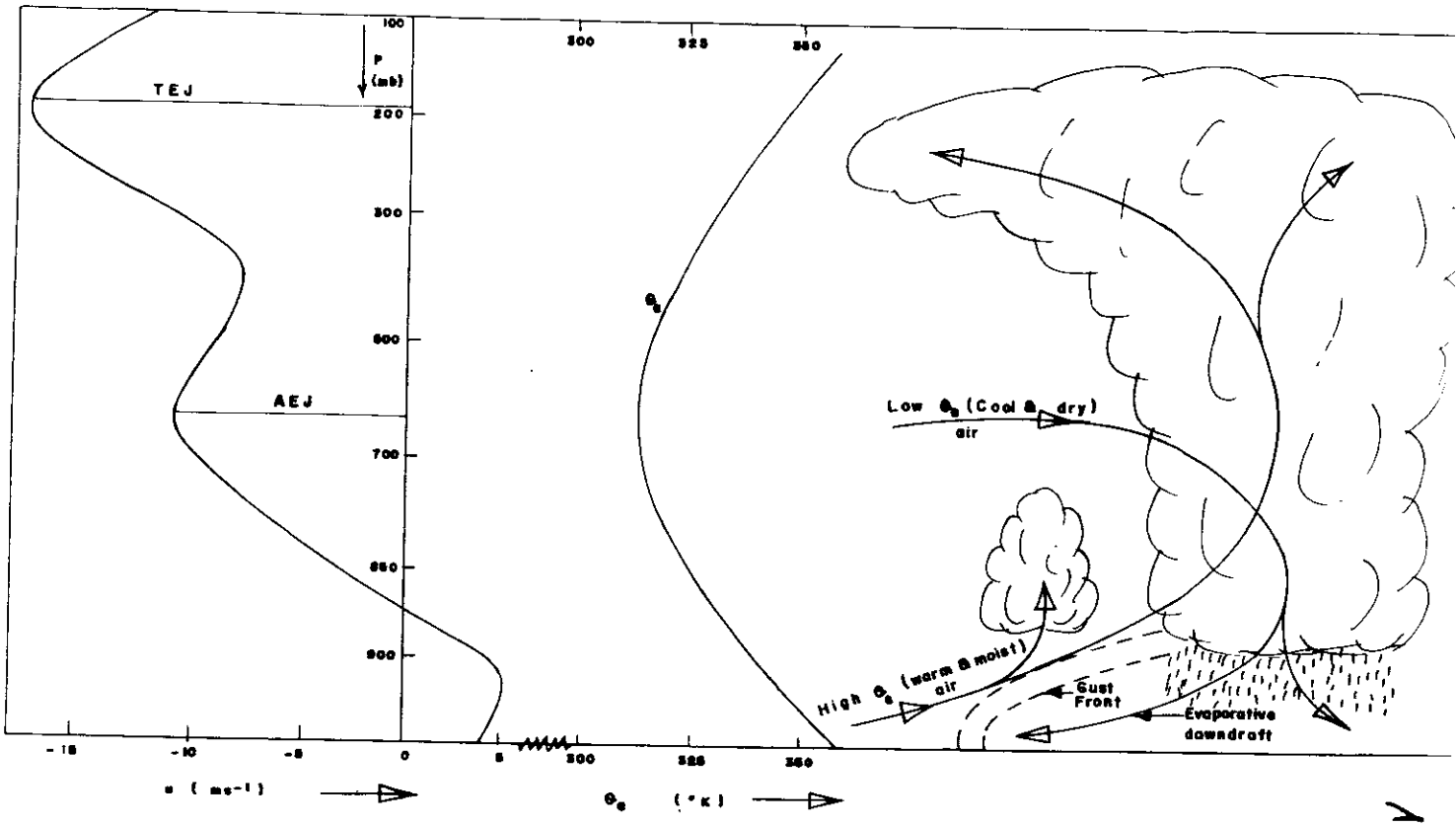

12

Fig. 13. The AEJ, θ_e & interaction with storm updraft / downdraft for Thunderstorm / Squall line sustenance.

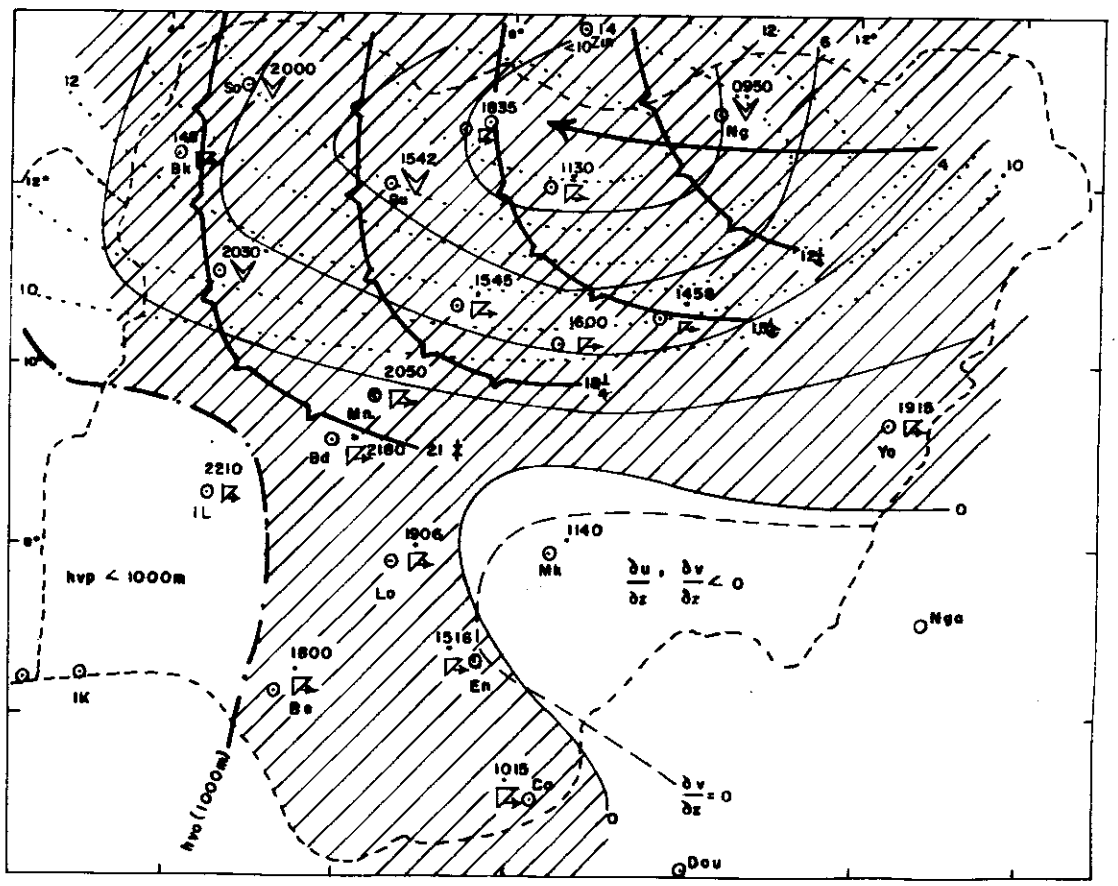

Fig. 14. Evidence of importance of simultaneous presence of positive boundary layer wind shear, at least One - Km deep moist layer and a well organised AEJ on widespread storm and line squall development (From Omotosho, 1984)

13

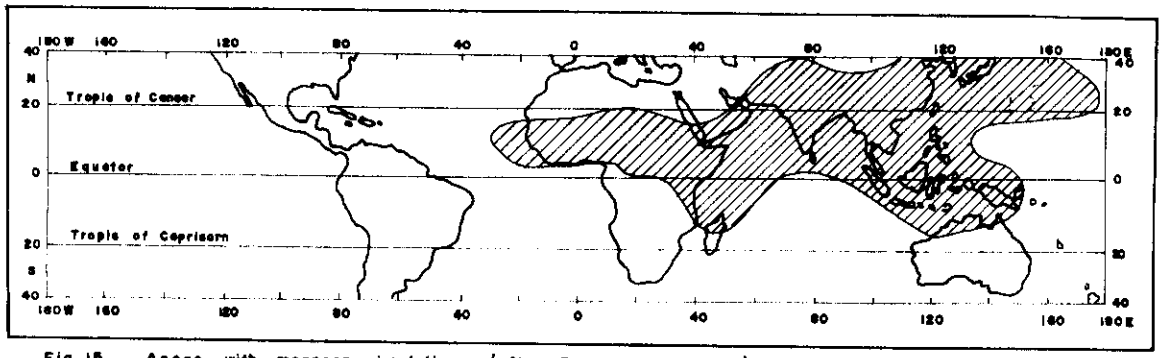

Fig. 15. Areas with monsoon circulations (after Ramage, 1971, p. 4)

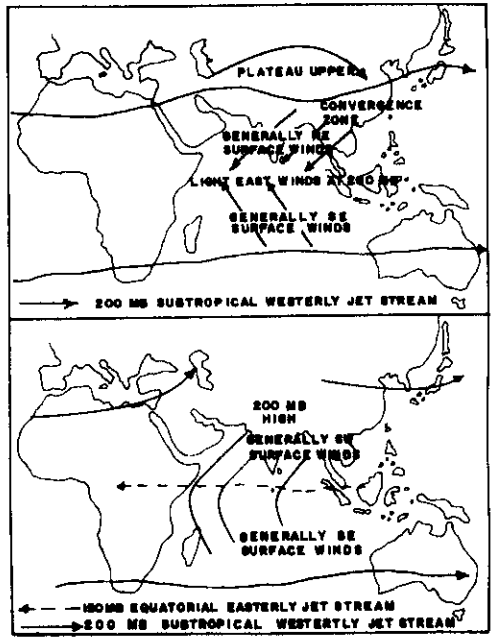

Fig. 16. Schematic illustrations of the major features of Asian monsoon. Upper: northern winter. Lower: northern summer. (Adopted from Lockwood, 1974)

16

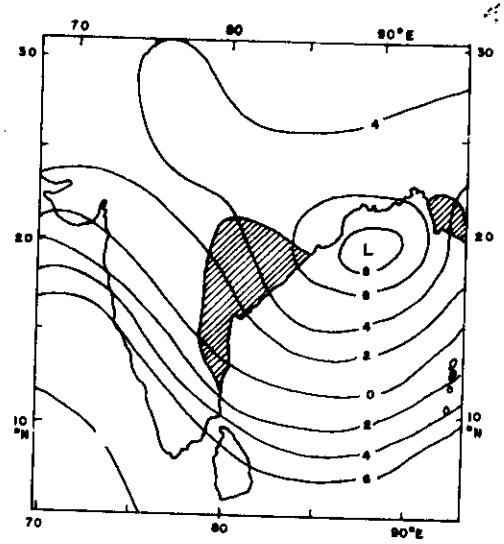

Fig. 17 An example of a monsoon depression over the Bay of Bengal. 1000-mbo contours in decametres for 12·00 GMT on August 20th, 1967. Hatched areas: continuous rainfall. (adopted from Nieuwolt, 1977).

17

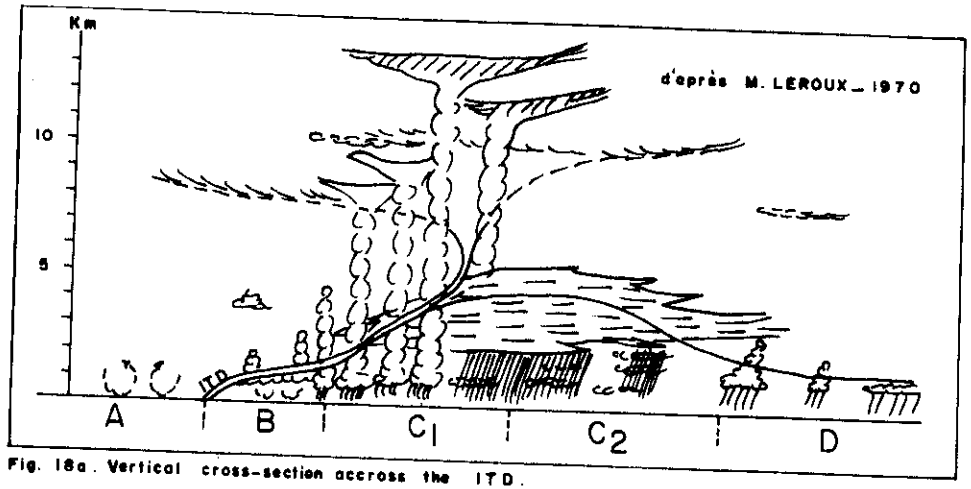

Fig. 18a. Vertical cross-section accross the ITD.

18

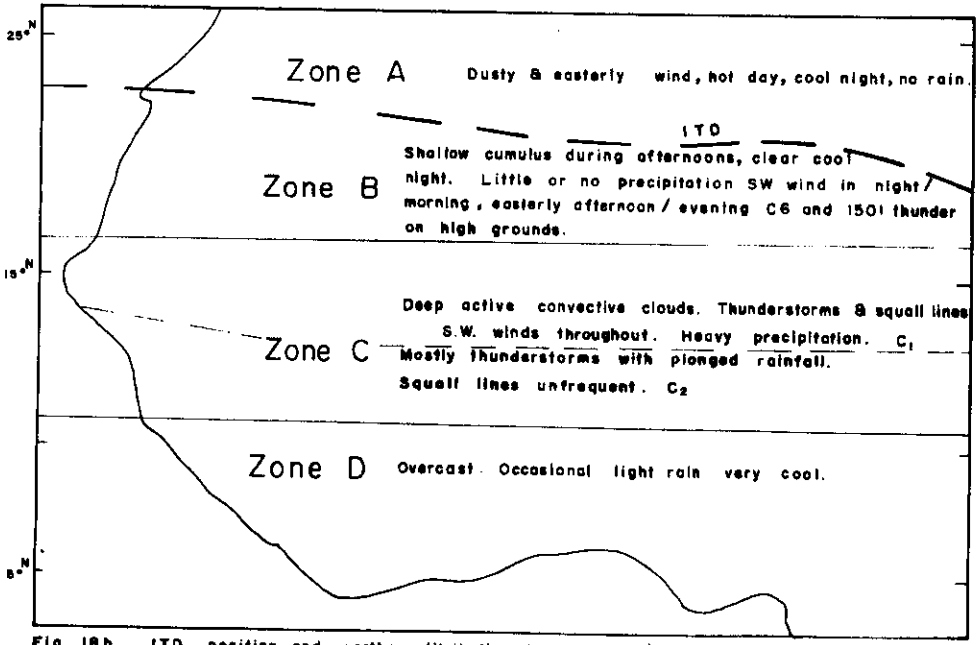

Fig. 18b. ITD position and weather ditribution in August. (most active weather is not where monsoon is deepest — compare Fig. 19.)

19

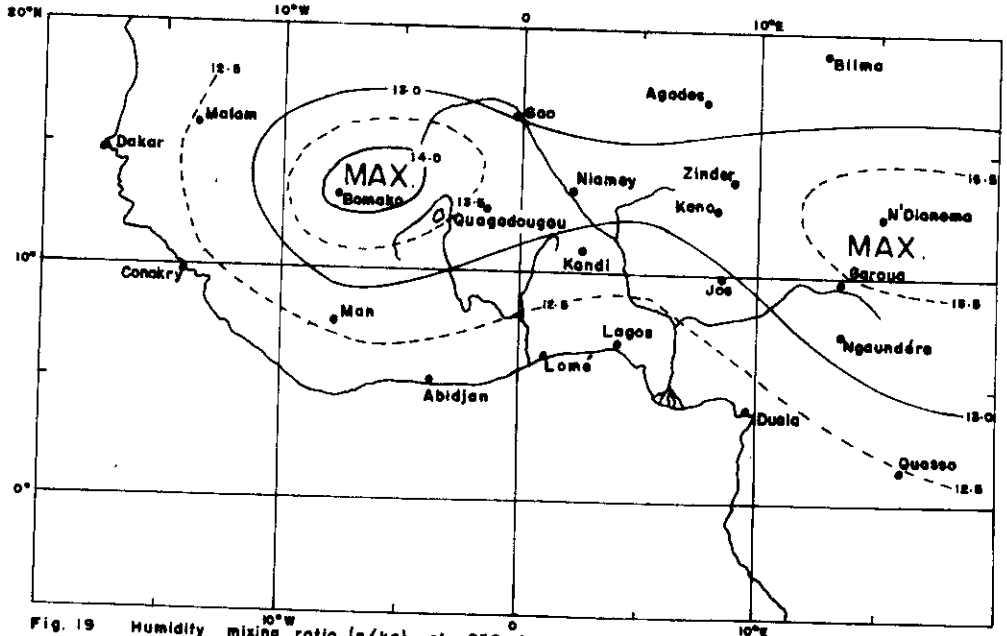

Fig. 19 Humidity mixing ratio (g/kg) at 850 mb in July. (from Omotosho 1976).

20

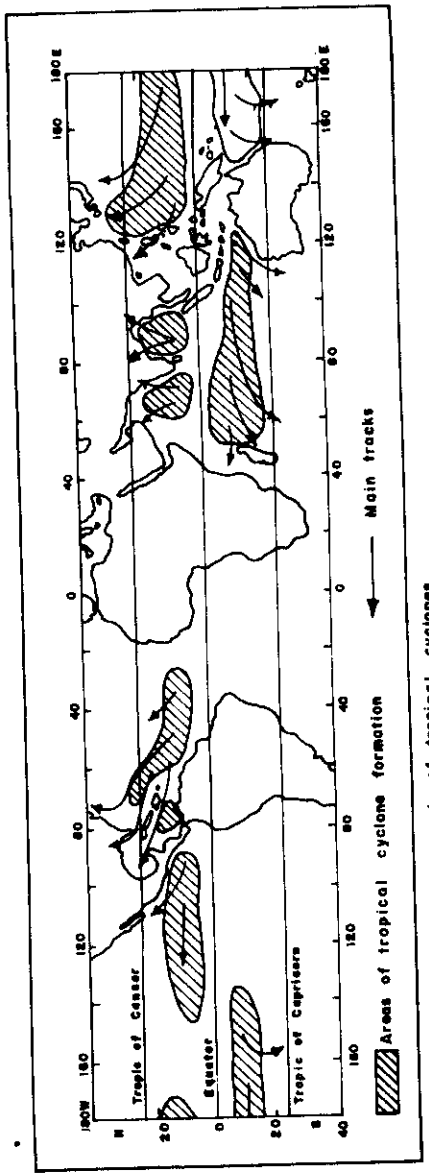

Fig. 20a Formation and movements of tropical cyclones

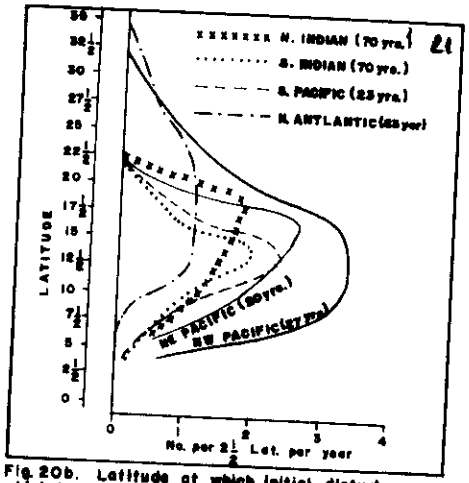

Fig. 20b. Latitude at which initial disturbances which later become tropical storms were first detected for the various development regions. Number of years in data average in parenthesis.

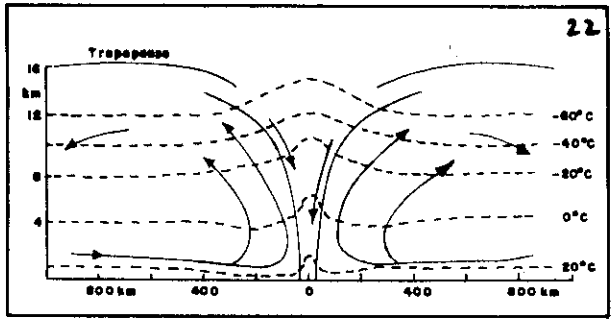

Fig. 21. Cross-section of a tropical cyclone. Vertical exageration about 50 times.

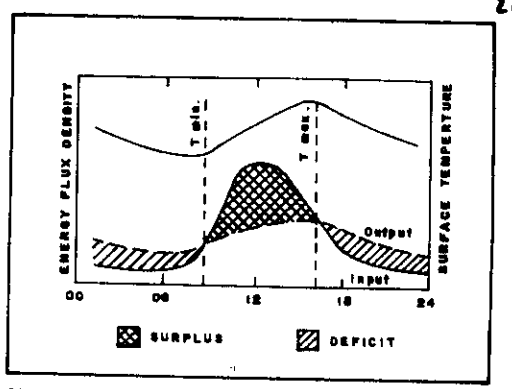

Fig. 23. The relationship between surface energy exchange and the diurnal surface temperature regime.

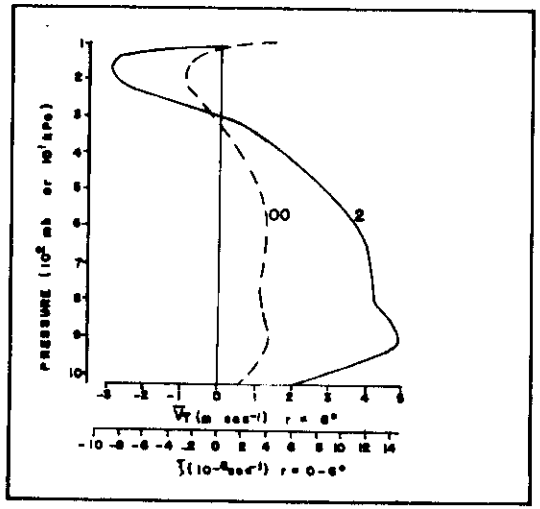

Fig. 22. Mean relative vorticity within the area r = 0-6° (equivalent to mean tangential winds in r = 6-7° band) from Zehr's (1976) developing (stage 2) and non-developing (stage 00) disturbances.

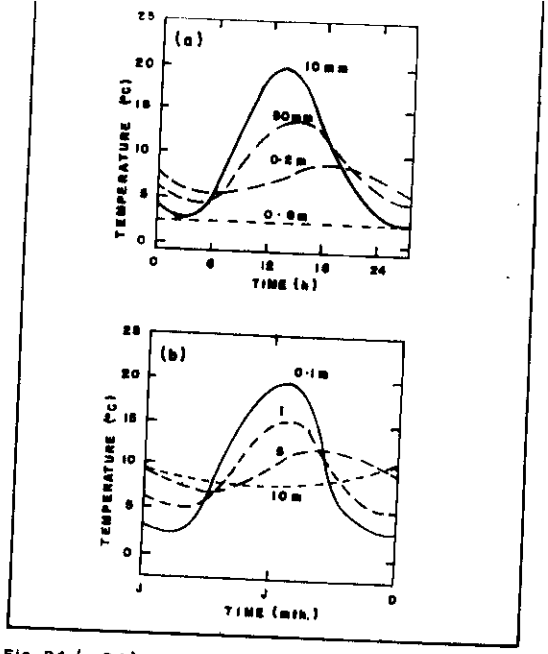

Fig. 24 (a & b). Generalized cycles of soil temperature at different depths for (a) daily and (b) annual periods.

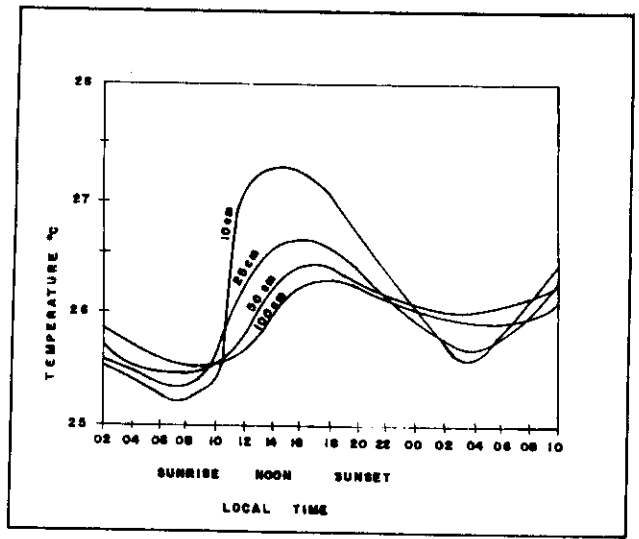

Fig. 24c Temperature variation below the ground at Ile-Ife, Nigeria. (after Babatunde & Balogun, 1983).

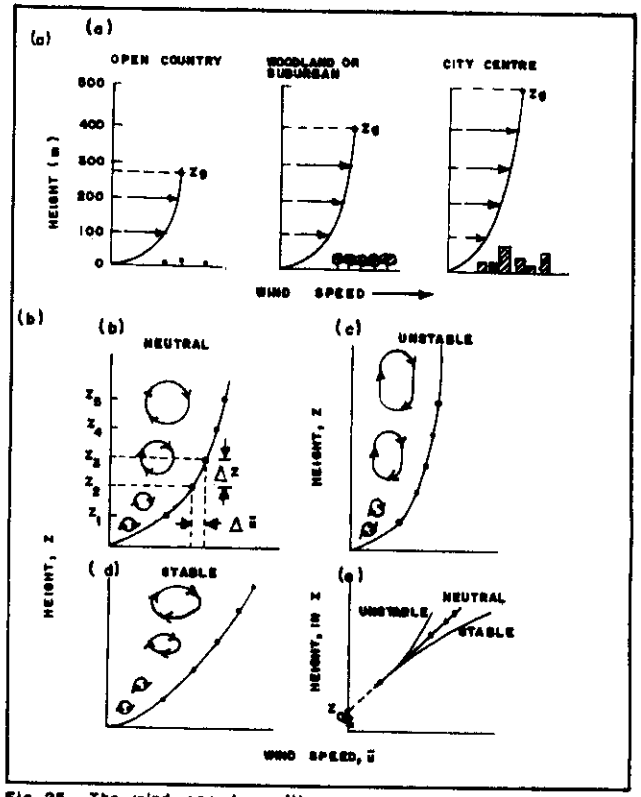

Fig. 25. The wind speed profile near the ground showing the effect of stability on profile shape and eddy structure.

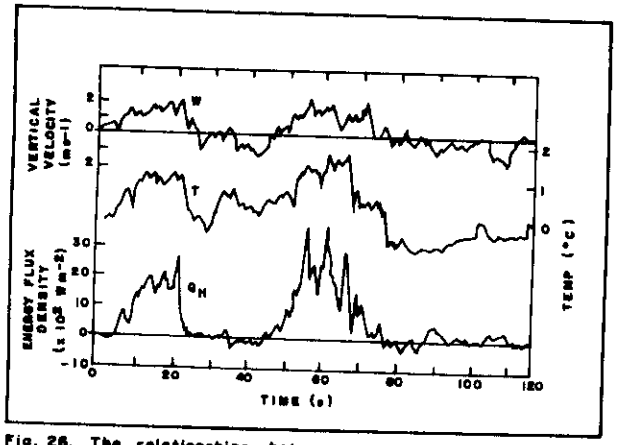

Fig. 26. The relationships between vertical velocity (w) and temperature (T) fluctuations, and the instantaneous sensible heat flux.

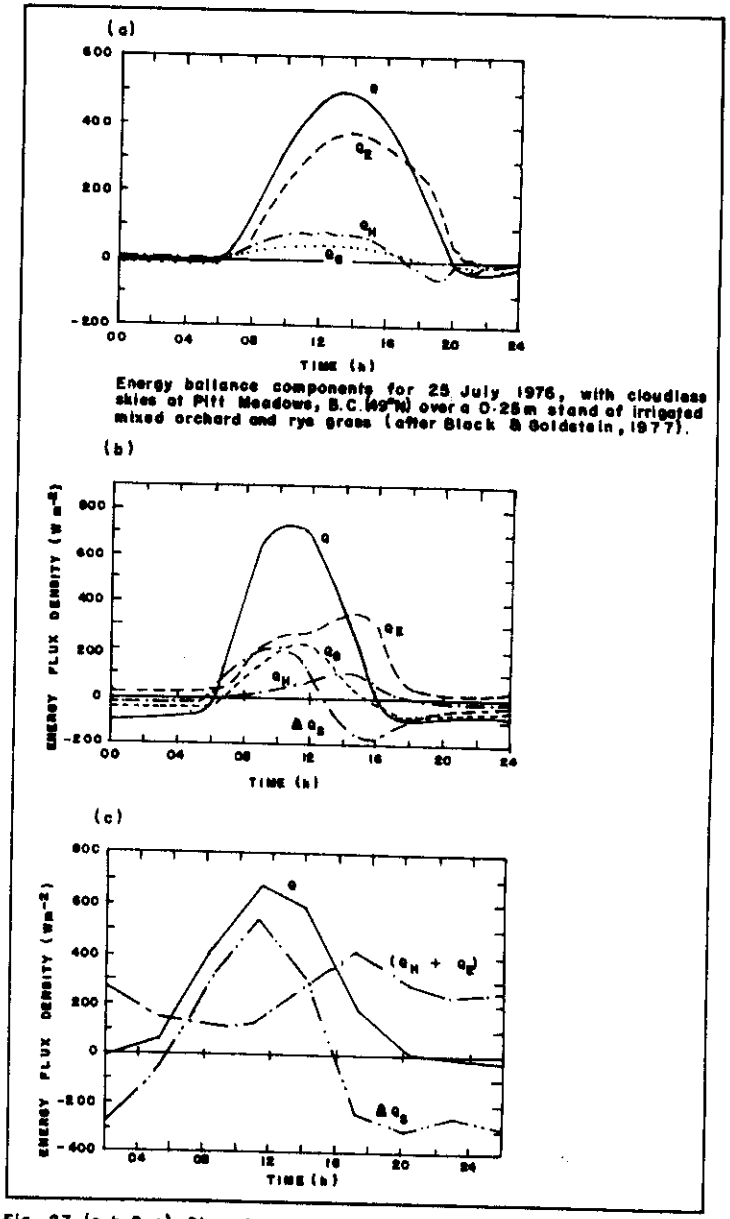

Energy balance components for 25 July 1976, with cloudless skies at Pitt Meadows, B.C. (49°N) over a 0·25m stand of irrigated mixed orchard and rye grass (after Black & Goldstein, 1977).

Fig. 27 (a,b & c) Diurnal variation of the energy balance components in and above (b) a shallow water layer on a clear September day in Japan (after Yabuki, 1957), and (c) the tropical Atlantic Ocean based on measurements from the ship Discoverer in the period 20 June to 2 July 1969 (after Holland 1971).